LOCATING UNMAPPED MINING VOIDS USING HIGH-RESOLUITION SEISMIC AND RESISTIVITY SURVEYS AT A HISTORICAL MINING AREA IN THE TRI-STATE MINING DISTRICT, QUAPAW OKLAHOMA

By

PATRICK MEESE

Bachelor of Science in Geology

Oklahoma State University

Stillwater, Oklahoma

2021

Submitted to the Faculty of the
Graduate College of the
Oklahoma State University
in partial fulfillment of
the requirements for
the Degree of
MASTER OF SCIENCE
December, 2021

LOCATING UNMAPPED MINING VOIDS USING HIGH-RESOLUITION SEISMIC AND RESISTIVITY SURVEYS AT A HISTORICAL MINING AREA IN THE TRI-STATE MINING DISTRICT, QUAPAW OKLAHOMA

Thesis Approved:

Dr. Ahmed Ismail

Thesis Adviser

Dr. Jim Puckette

Dr. Todd Halihan

ACKNOWLEDGEMENTS

Sanuade, Oluseun

Sazal, Md Zonaed Hossain

Name: Patrick Meese

Date of Degree: DECEMBER, 2021

Title of Study: LOCATING UNMAPPED MINING VOIDS USING HIGH-RESOLUITION SEISMIC AND RESISTIVITY SURVEYS AT A HISTORICAL MINING AREA IN THE TRI-STATE MINING DISTRICT, QUAPAW OKLAHOMA

Major Field: Geology

Abstract: The Tri-State Mining District in northeast Oklahoma has been heavily undermined, leaving both large and small manmade void spaces that pose a danger to both property and human life. The district is classified as the Tar Creek Superfund Site due to the combined hazards of toxic levels of zinc, cadmium and lead in mine waste, soil, air, and water. The underground voids present an additional hazard for subsidence due to extensive undermining. This study tested the effectiveness of the seismic land streamer and resistivity Ohm Mapper geophysical tools for providing high-resolution seismic and electrical resistivity images of mining voids at the study site. The seismic land streamer and resistivity Ohm Mapper were selected in this study because they enable rapid data acquisition with minimum interaction with the ground surface and require a small crew to acquire data. The acquired seismic data were analyzed as P-wave reflection, refraction, and multichannel analysis of surface wave. These were used to generate multiple profiles of the subsurface and maximize the chance of detecting mining voids. The results showed that the Ohm Mapper resistivity images were ineffective in detecting mining voids due to the high noise level in the data and the limited imaging depth. However, the seismic land streamer images successfully detected multiple mining voids along the acquired profiles. This study of the Tar Creek Superfund Site demonstrated that a seismic land streamer is an effective tool for acquiring suitable data to characterize subsurface voids.

TABLE OF CONTENTS

LIST OF TABLES

Table Page

LIST OF FIGURES

Figure Page

CHAPTER I

INTRODUCTION

The detection of subsurface mining voids is important for evaluating the potential for subsidence in populated areas and for the safety of geotechnical designs, buildings, roads and bridges. Several geophysical techniques are used to map mining voids including but are not limited to electrical resistivity tomography (ERT) (Bharti et al., 2016) ground penetrating radar (GPR) (Nobes, 2017), and seismic (Miller and Steeples, 1991) methods. The effectiveness of these methods to detect subsurface mining tunnels depends on the difference in the physical properties between the materials that fill the voids left by mining and the host rocks.

GPR could be a highly accurate and reliable geophysical technique to image voids, however, the depth of penetration is not sufficient to be useful in many cases, especially when the near surface materials are rich in clay. The ERT is typically used for identifying void spaces such as mining tunnels as it is reliable, and can image deep into the subsurface. However, the ERT method is difficult to use in residential and urban areas where significant portions of the ground surface is covered by concrete, asphalt, and

the subsurface. However, the ERT method is difficult to use in residential and urban areas where significant portions of the ground surface are covered by concrete, asphalt, and other structures as ERT requires drilling through these hard surfaces to sink the electrodes into the ground (Sheets, 2002).

The subsurface imaging of voids created by mining tunnels requires a geophysical method that could provide high resolution images as well reasonable depths of penetration (Ding et al., 2021). Seismic methods are used to detect subsurface voids created by mining tunnels. Some of the seismic techniques that have been utilized for the detection of voids include multichannel analysis of surface wave (MASW), seismic P-wave refraction, and seismic P-wave reflection (Ivanov et al., 2016; Filippi et al., 2019; Ding et al., 2021). Recently research has grown in using surface waves in detecting voids using MASW, Rayleigh-wave diffraction, backscattered surface waves, and attenuation (Ding et al., 2021). Xia et al. (2006) and Zeng et al. (2009) used synthetic models to demonstrate the application of diffracted Rayleigh waves to resolve subsurface voids. Chai et al. (2012) through the research of Rayleigh wave scattering, it was possible to establish a link between wavelength and cavity depth.

Seismic refraction methods were also used to detect voids over 10 meters at different geological settings. McCann et al. (1982) used first arrival times of refracted P-waves to detect a 5 meter (m) diameter tunnel at 9 m depth. Refraction tomography was employed by Belfer et al. (1998) to identify the tunnel location as a limited low-velocity zone. Riddle et al. (2010) detected an engineered tunnel of 1.0 m × 1.6 m in size and approximately 6 m deep using refraction tomography.

The P-wave seismic reflection method has the potential to overcome the limitations of the GPR and the ERT methods and can be an effective approach if mining tunnels are located orthogonal to the seismic survey lines. P-wave seismic reflection surveys utilizing a sledgehammer as a source and a set of 24 geophones can penetrate down to ~50 m depth to image deep mining voids. Surveys using a sledgehammer source and a seismic land streamer system, a series of geophones secured to plates and secured together on Kevlar webbing, have the advantage of not needing to plant the geophones into the ground. These surveys can cover large distances rapidly and require a small field crew, thereby minimizing the number of people necessary to acquire data. With an automated source, a single person could conceivably cover a 2 km length profile in 8 hours. Furthermore, as the land streamer system does not need planting geophones into the ground during data acquisition, it can easily be pulled along paved roads or streets in any urban area where the surface is covered in concrete, asphalt, or brick.

Some factors can pose significant challenges to the applications of geophysical methods for detecting voids including the depth and size of the voids, nature of the ground surface and any environmental hazards that may pose a health risk to workers at the sites being surveyed. The study area at the Tri-State Mining District was selected in part due to the fact that it is now, the Tar Creek Superfund Site. The Tri-State Mining District is a region that was heavily mined for lead and zinc at relatively shallow depths and this process left underground voids close to the surface and hazardous levels of toxic compounds in mining waste in the form of tailing piles and mill ponds. The piles of waste rock called "chat" were used as road and driveway material and contributed to the widespread contamination of soil that contributed to significantly elevated lead levels in the residents

of Picher, Oklahoma (United States Army Corps of Engineers, 2006). While the short-term exposure of the geophysics survey team to conditions at the site may not pose a health threat, exposing a team to hazardous conditions for any length of time is less than ideal.

Despite the fact that seismic methods have proven to be effective for detecting subsurface voids, the use of a single geophysical method in the detection of voids may not provide a reliable characterization of the voids. This is largely due to the variability in the geometry of voids. The use of multiple geophysical methods (e.g. seismic and electrical methods) will minimize the non-uniqueness in the geophysical data interpretation for voids. Seismic methods, for example, will be able to provide information on the mechanical properties of subsurface materials, while electrical methods will be able to provide information on the moisture content of subsurface materials. Hence, the integration of seismic and electrical methods will provide a detailed imaging of voids in the subsurface.

The main goal of this research is to test the efficacy of the P-wave seismic reflection using the seismic land streamer technology and the electrical resistivity method using the OhmMapper (OM) system for detecting mining tunnels voids at a superfund site. The study will also evaluate the usefulness of analyzing the acquired P-wave reflection data as refraction and MASW images to maximize the benefit of the single seismic survey for detecting mining voids. This study compares and integrates the electrical resistivity images and the multiple seismic images for a better detection of mining voids at the surveyed sites.

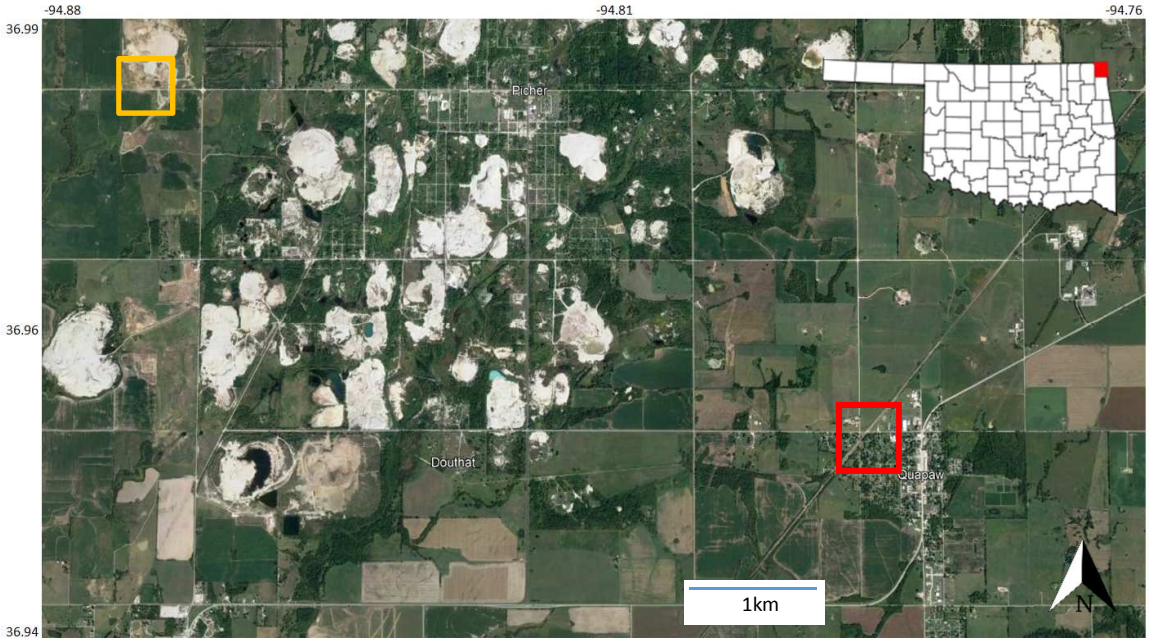

Figure 1. Location of the primary study area in Quapaw, Oklahoma (red box), and the secondary location west of Picher Oklahoma (orange box). The grey/white areas are tailings piles.

CHAPTER II

SITE DESCRIPTION

The Picher Mining field within the Tri-State Mining District in northeast Oklahoma was an active mining area from 1904 to 1970. The area was declared a superfund site in 1983 due to the combined hazards of toxic levels of zinc, cadmium and lead in the air, soil and water as well as the danger of subsidence due to extensive undermining of the area including the communities of Cardin and Picher. Despite the extensive efforts to remove the chat piles, massive mounds of mining waste still remain on the surface (figure 1). Chat piles continue leaching toxins into the groundwater aquifers as well as fine grained material with in the chat and mill ponds being blown around by the wind. Remediation of the subsurface is an ongoing task (United States Army Corps of Engineers, 2006).

In 2004, Oklahoma U.S. Senator Jim Inhofe requested an evaluation for the potential of major subsidence in the area. A subsidence evaluation team led by the U.S. Army Corps of Engineers was formed to complete the proposed project and evaluate the potential for subsidence in the Tri-State Mining District. This group came to the conclusion that

subsidence caused by shafts and mining tunnels posed a serious concern to the well-being of those who live and travel in the vicinity. Although some residential and high traffic areas, including major roadways, are prone to some level of subsidence, the group did qualify this by highlighting that the area vulnerable to subsidence makes up a small fraction of the overall study area. (United States Army Corps of Engineers, 2006).

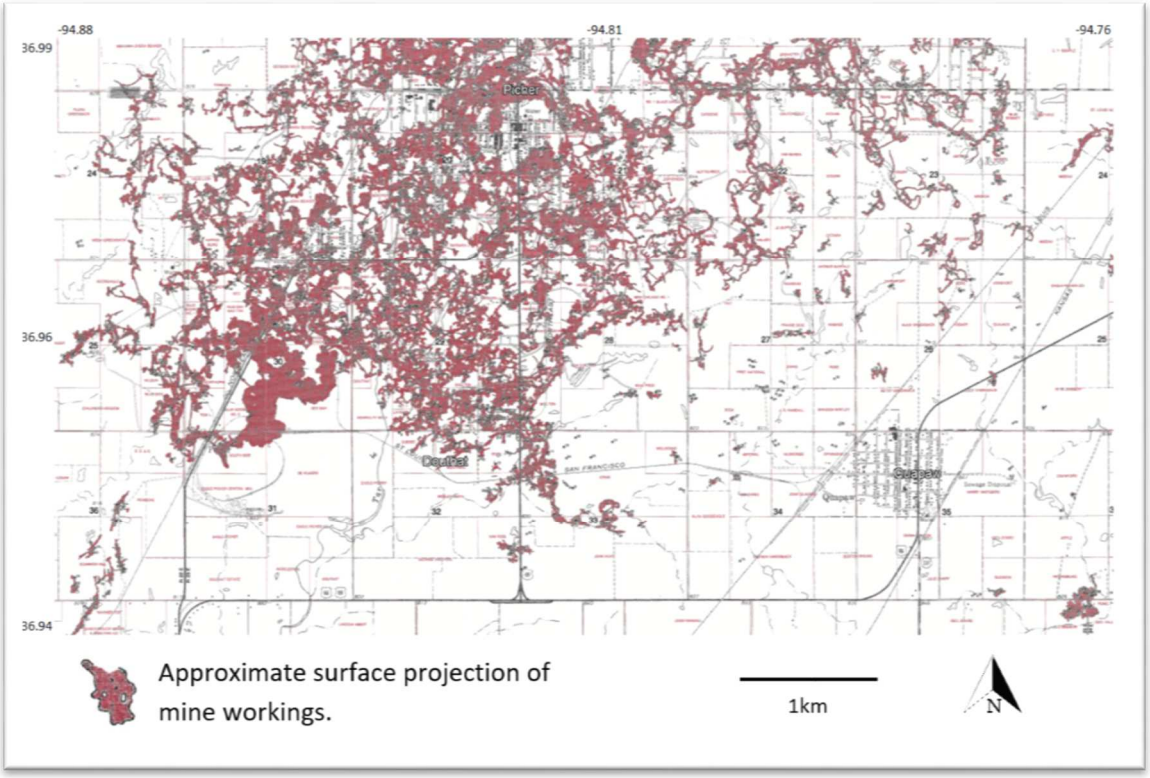

Figure 2 Map showing the recorded mining that took place in the Picher Field of the Tri-State Mining District. Modified from Luza (1986).

The group released a report in 2006 and efforts are being made to mitigate the subsidence potential in many areas in the Tri-State Mining District. There was however a gap in their findings. While mining documents suggest that the cities of North Miami and Commerce in the Tri-State Mining District were not seriously undermined, blueprints for mines

beneath the city of Quapaw were not located, according to the report. The location of the mineshafts is the only known information about these mines. Due to the missing mine data, exactly how much undermining of the town of Quapaw occurred is unknown (United States Army Corps of Engineers, 2006).

Subsidence is not only an issue in areas where there are known mining tunnels or subsurface tunneling. The need to quickly and efficiently scan a built-up area for unknown void spaces is a hole in the geophysical community's current methods that needs to be filled.

Geology

The geology and origin of the lead and zinc deposits in the Tri-State Mining District has been discussed by multiple authors since the early 20th Century including Brockie et al. (1968), and McKnight and Fischer (1970). The Mississippian and Pennsylvanian rocks exposed at the surface in the mining area reveal a relatively flat structure with a 4 meter per kilometer regional northwestward dip. In deep boreholes and wells in this region Cambrian and Ordovician formations composed primarily of dolomites, chert and some sandstone with minor shales are present, though as they do not pertain to this study they will not be covered. (Luza, 1986)

The main host of lead and zinc ore is the Boone Formation, which is mainly composed of fossil limestone and thick layers of nodular chert (Luza, 1986). The Boone Formation

in the Picher, Oklahoma area is between 100 and 125 m thick and is partitioned into seven members (in descending order): Moccasin Bend, Baxter Springs, Short Creek Oolite, Joplin, Grand Falls Chert, Reeds Spring, and St. Joe Limestone (McKnight and Fisher, 1970). As illustrated in figure 3, Fowler (1942) further separated these members into 16 beds, which he identified using letters of the alphabet, starting with B at the top of the Moccasin Bend member and ending with R in the Reeds Springs member. The ore deposits in the Picher mining field are mostly found in the top part of the Boone Formation, with the M bed accounting for the majority of them (figure 3) (McKnight and Fisher, 1970). Ore was also found in the K, G, H and E beds (McKnight and Fisher, 1970). Ore bodies found in the region consist mainly of flat masses that run horizontally over large distances and are largely confined to stratigraphic intervals and exhibit parallel margins (Luza, 1986).

Table 1. Lithological description of a water well near the surveyed area.

MULTI-PURPOSE WELL COMPLETION & PLUGGING REPORT
WELL ID NUMBER: 149823 Ottawa Ok.
Firm Name WHISNER WELL DRILLING Drilled to a depth of: 624 feet
Latitude 36.965347585 Longitude -94.8037355

Material	From (feet)	To (feet)
Overburden	0	2
Clay and Mud	2	35
Limestone	35	80
Shale	80	85
Limestone with interbedded chert.	85	624 Bottom not located

Based on limited available information on the geology in the Quapaw area, the topmost layer encountered is likely the Pennsylvanian Hartshorne shale at a depth of about 5 m. This is a well-laminated shale, however, at the Quapaw site; it is believed to only be roughly 2 meters thick as the site is located on the terminating edge of this formation. Below the Hartshorne Formation are the Mississippian Batesville and Hindsville formations, which based on logs obtained from water wells in the area are primarily limestone with some interbedded mudstone and chert (Luza, 1986). The principal ore-bearing Mississippian Boone Formation is encountered consisting primarily of limestone and cherty limestone (Table 1).

System	Series	Group, Formation, or member		Bed
PENNSYLVANIAN	Desmoinesian	Krebs Subgroup (Cherokee Group)	Boggy Formation Bluejacket Sandstone Member	
			Savanna Formation Doneley Limestone Member (Reed and others, 1955)	
			McAlester Formation Warner Sandstone Member Hartshorne Formation McCurtain Shale Member	
MISSISSIPPIAN	Chesterian	Fayetteville Shale		
		Batesville Sandstone		
		Hindsville Limestone		
	Meramecian	Quapaw Limestone		
		Boone Formation	Moccasin Bend Member	B C D E F G H
			Baxter Springs Member	J K L
			Short Creek Oolite Member	
	Osagean		Joplin Member	M
			Grand Falls Chert Member	N O P Q
			Reeds Spring Member	R
	Kinderhokian and Upper Devonian		St. Joe Limestone Member	
MISSISSIPPIAN and DEVONIAN		Chattanooga Group		
ORDOVICIAN	Lower Ordovician	Cotter Dolomite Jefferson City Dolomite Roubidoux Formation Gasconade Dolomite Gunter Sandstone		
CAMBRIAN	Upper Cambrian	Eminence Dolomite Potosi Dolomite Derby-Doe Run Dolomite Davis Formation Reagan Sandstone		
PRECAMBRIAN		Granite and volcanics		

Figure 3 Generalized stratigraphic column for the Tri-State Mining District (Luza, 1986)

CHAPTER III

METHODOLOGY AND DATA

P-wave Seismic

Four high-resolution seismic(HRS) P-wave profiles marked as Lines 1, 2, 3, and 4, were acquired along two east-west streets as well as two north-south street in Quapaw, Oklahoma (Fig. 5a). A fifth line marked as Line 5, was acquired over a known void produced by mining along a dirt road north of the ghost town of Picher, Oklahoma (Fig. 5b). A P-wave seismic land streamer consisting of 24 - 40Hz geophones vertically mounted on metal plates was used to acquire this data. These plates are secured together at 2 m intervals using special Kevlar reinforced webbing that resists stretching. A 10 kg sledgehammer striking a 2-inch-thick steel plate vertically was used as a source spaced at 2 m from the first geophone. Acquisition parameters are summarized in Table 2.

Data for Lines 1, 2, 3 and 4 were acquired in a sparsely populated residential area on the edge of the small town of Quapaw, Oklahoma. These four profiles were collected along paved roads that allowed for good coupling with the land streamer sleds and the ground. Care was also taken to no collect data while no vehicular traffic was passing nearby and

due to the sparsely populated nature of the area, this was not a common issue. The weather during the acquisition of data for lines 1, 2, and 3 was fair and the wind was low, resulting in little to no reduction in the quality of the data. Line 4 was acquired during light rain and higher winds of about 24 mph however these weather conditions do not seem to have affected the quality of the data as shown in figure 6.

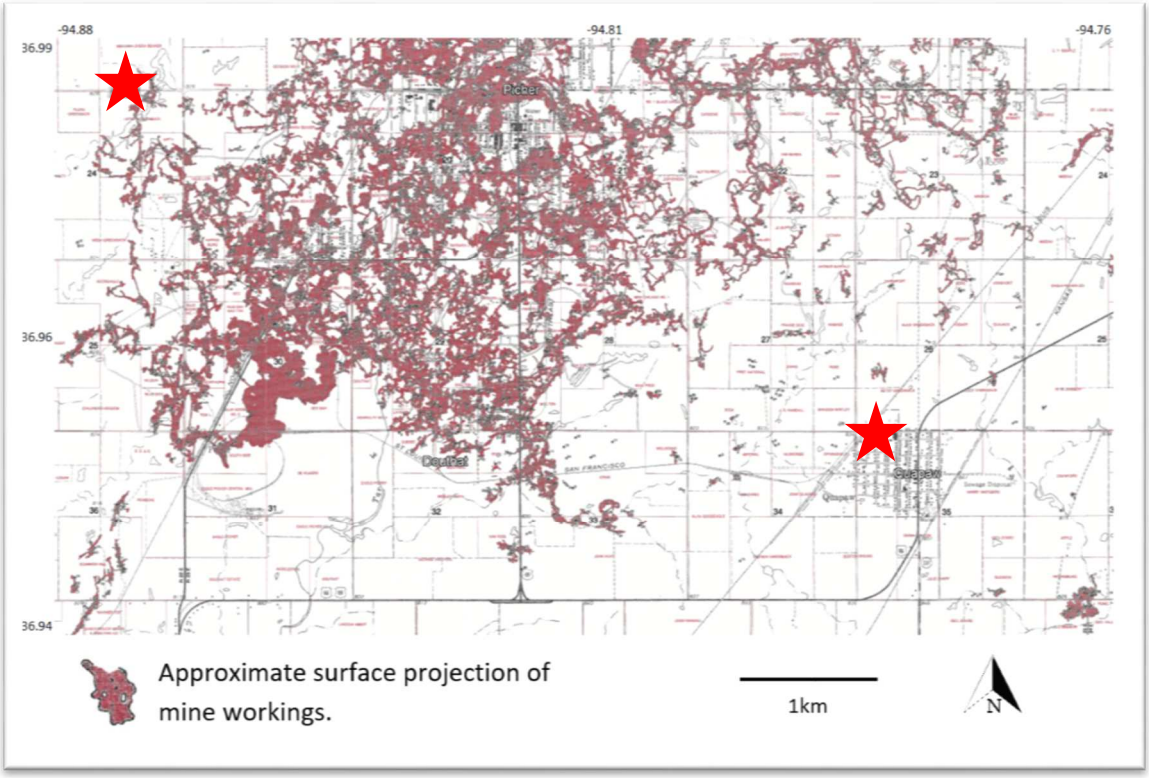

Figure 4. A map of the Tri-State Mining District showing the locations of the two study sites labeled with red stars.

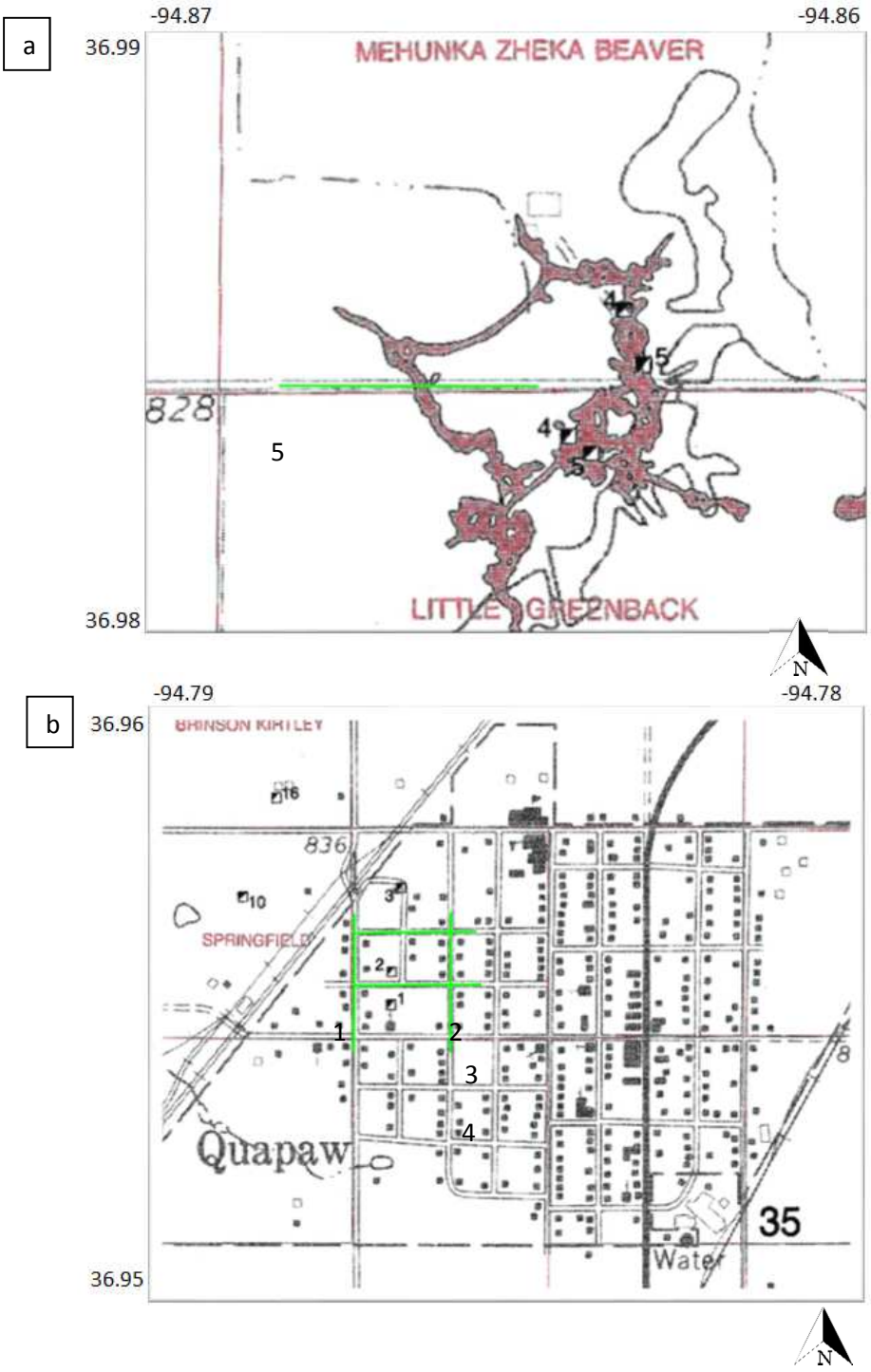

Figure 5 Maps of the study site west of the town of Picher (a) and within the town of Quapaw (b), showing locations of the conducted P-wave seismic reflection and capacitively coupled resistivity surveys.

Table 2. P-wave seismic data acquisition parameters

Data Collection Parameters	
Parameters	
Channels	24
Geophone type	Vertical 40 Hz
Source type	10 lb Sledge hammer
Geophone interval	2 meters
Source interval	2 meters
Stack	3
Sampling rate	0.5 milliseconds
Record length	1.0 seconds
Recording system	Geode

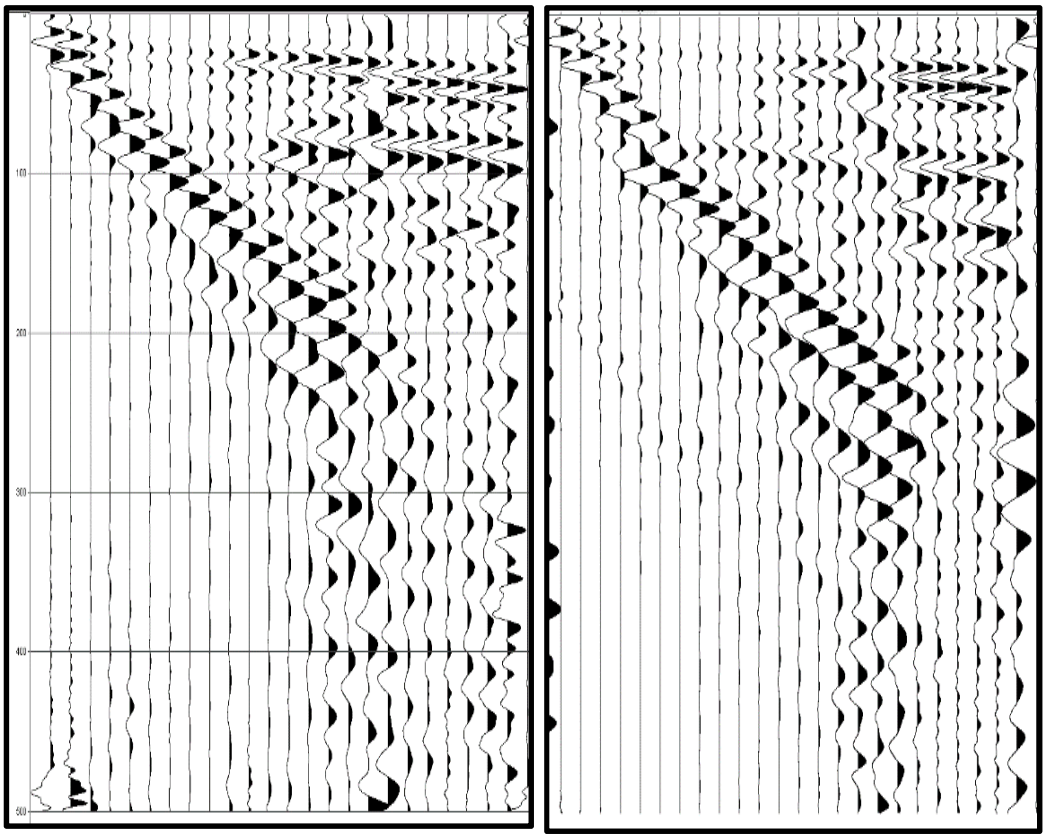

Figure 6 Examples of randomly selected P-wave shots from initial data collection

The acquired P-wave reflection data were analyzed and processed as P-wave refraction and multichannel analysis of surface wave (MASW) along the reflection profile. Although, it is recommended that low frequency (4.5 Hz) geophones be used for the MASW data acquisition, we used 40 Hz geophones in this study and obtained a good Rayleigh wave.

Capacitively Coupled Resistivity Method, OhmMapper

The resistance to the flow of electric current in a specific material is referred to as resistivity. The voltage difference between two potential electrodes is measured after injecting a known current into the ground using two current electrodes. The resistance can be determined using Ohm's law by dividing the observed voltage by the transmitted current.

The capacitively coupled resistivity systems application when traditional resistivity methods proved to be challenging or impossible (Geometrics, 2018). This includes areas covered with thick ice, snow, concrete or asphalt. This system injects current capacitively into the Earth through a line antenna and measures the potential difference in the same way (Geometrics, 2018). According to Geometrics the capacitively coupled resistivity system has limitations in areas that are electrically noisy or with subsurface compositions that are highly conductive. With the latter issue, it is very difficult to inject currents into the ground in this manner when compared to a conventional resistivity system (Geometrics, 2018). Current is transferred into the ground in CCRS surveys by using

capacitance. This allows the system to collect data faster and more efficiently without the need for electrodes to be in direct contact with the ground (Geometrics 2018). The ground and the wire in each dipole cable operate as opposing conductor plates of a capacitor, with the air between dipole cables in the ground acting as an insulator between the plates (Geometrics, 2001).

The Geometrics OhmMapper is a capacitively coupled resistivity meter that allows the electrical characteristics of rock and soil to be measured without the need of standard electrodes. A basic array with transmitter and receiver sections is towed along the ground by a single person or coupled to a compact all-terrain vehicle, collecting data much faster than traditional DC resistivity survey methods. One major advantage of the system is that it allows for multiple passes using different transmitter and receiver spacing to build a finely sampled image of the subsurface (GeoMetrics, Inc, 2001). The OhmMapper is capable of axial dipole-dipole resistivity surveys typically to a depth of investigation between 10 and 20 m. Furthermore, the receivers will automatically sync to the transmitter cycle enabling offsets to be quickly modified in the field without major adjustments to allow for multiple depths of investigation (GeoMetrics, Inc. 2001). Capacitively coupled systems like the OhmMapper give us the advantage of not requiring electrodes to be sunk into the ground as traditional ERT systems do. As with traditional ERT systems the OhmMapper is able to produce profiles of the sub surface down to a depth of 15m under ideal conditions, as well as imaging horizontal variations in the near surface. This means that they can be also be used on compacted surfaces as well as on concrete and asphalt that would eliminate traditional ERT methods. OM systems show

promise for archaeological applications, however they sufficient spatial resolution and sensitivity for detailed studies.

Capacitively coupled resistivity data sets were acquired in the summer and fall of 2021 using a Geometrics OhmMapper (Geometrics, Inc. San Jose, Ca. U.S.A.), which was towed behind a vehicle. The system was set up in a configuration with 5 receiver dipoles each consisting of a pair of 5 m antenna cables coupled to each end of a receiver unit creating a dipole length of 10 m. The dipole length is matched on the transmitter which is placed at the rear of the array and is connected to the receivers via a non-conductive rope (Geometrics, 2001).

Figure 7. Field photos of electrical resistivity data acquisition (left) and seismic data acquisition (right).

CHAPTER IV

DATA PROCESSING

Multichannel Analysis of Surface Wave (MASW)

The steps involved in processing MASW data are shown in Fig. 8. For the pre-processing, the field data format (.dat) is converted to the Kansas Geological Society (KGS) format in the SurfSeis software. Thereafter, acquisition geometry such as surface coordinates of source and receivers were assigned to the data prior to the main processing analysis.

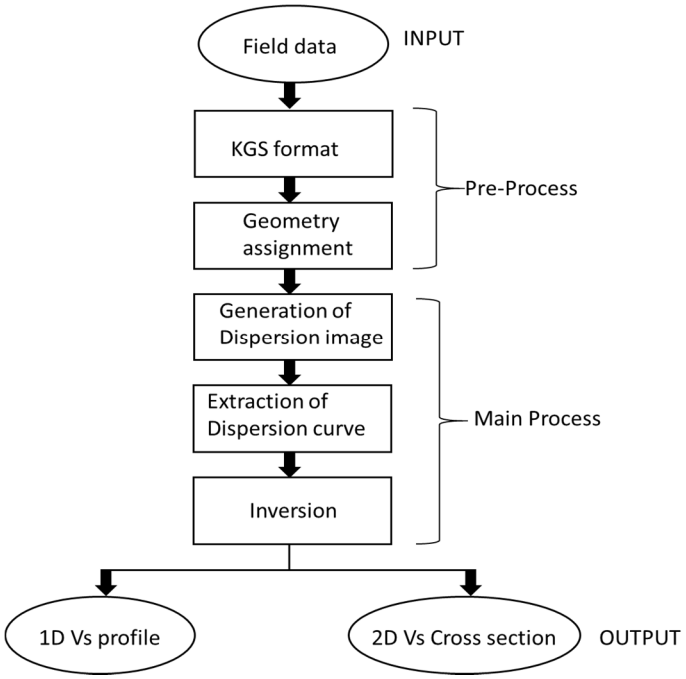

Figure 8: Flow chart showing the processing sequence of the MASW data.

The first step in the main processing of the MASW data involves the conversion of the acquired data shot gather from time to frequency domain using Fast Fourier Transform. The dispersion properties of the surface waves were then imaged by using a method FK transform (Ivanov et al., 2015). The individual multichannel record was converted into overtone (dispersion curve image) which shows diverse dispersion patterns. Thereafter, the fundamental mode of the Rayleigh wave, which are dispersion features, were interpreted and estimated based on the trend of the energy (Fig. 9). The point selected on the dispersion curve (Fig. 9) were inverted to generate a 1D shear wave velocity (Vs) converting the data shot gather from time to frequency domain using Fast Fourier Transforms profile. The purpose of this inversion is to obtain a velocity layer model that matches the calculated dispersion curve and observed dispersion curve points (Fig. 10).

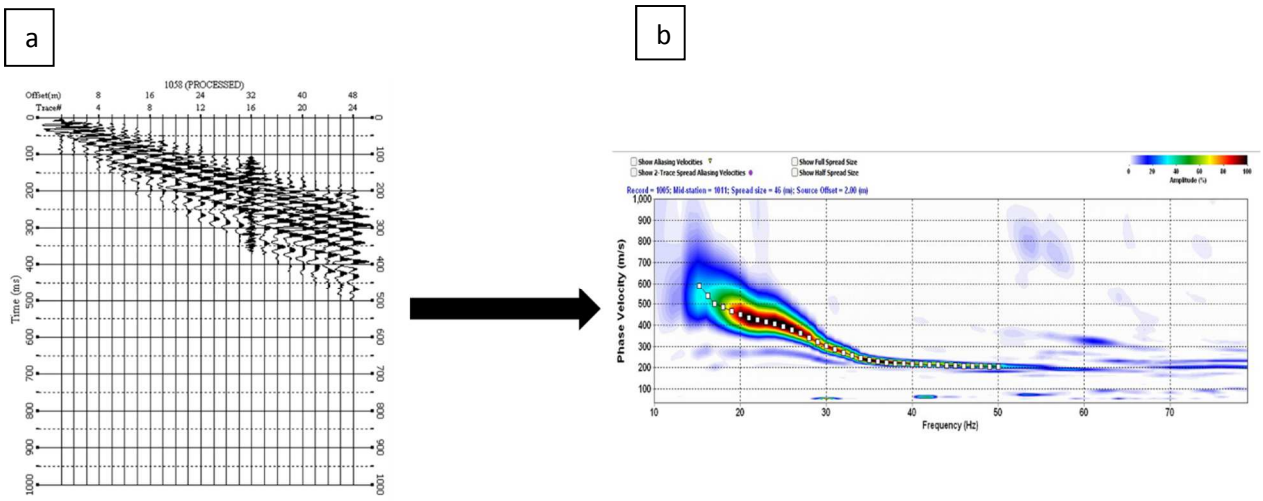

Figure 9: An example seismic shot record (a), and the generated dispersion curve image from the seismic record (b).

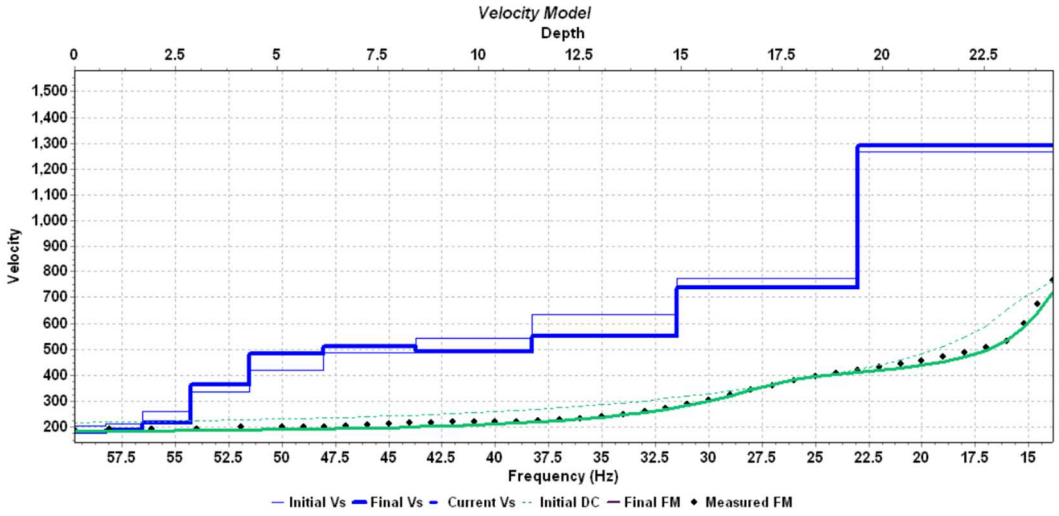

Figure 10: Inversion of the picked dispersion curve from figure 9b. The black dots represent the measured dispersion curve. The thin blue step is the initial Vs model; the thin green dashed line is the calculated dispersion curve from the initial Vs layer. The thick blue step represents the final Vs model while the thick green line is the calculated dispersion curve from the final Vs model.

The process of inversion begins with an initial Vs model which was used to calculate the dispersion curve. The calculated dispersion curve was then compared with the measured (picked) points on the dispersion curve. The inversion algorithm (least square approach) used the difference between the measured and the calculated dispersion curve to estimate a modification of Vs model in order to obtain a new Vs model. The new Vs model was then used to obtain another dispersion curve. The new dispersion curve is then compared to the dispersion curve that was picked in an iterative process. This iteration process proceeds until the calculated dispersion curve matches the dispersion curve that was picked (Fig. 10). The final step involves the assembling of several 1D Vs profiles to obtain a 2D Vs model (Fig. 11). The surface location of each 1D Vs profile was estimated using the middle of the receiver spread.

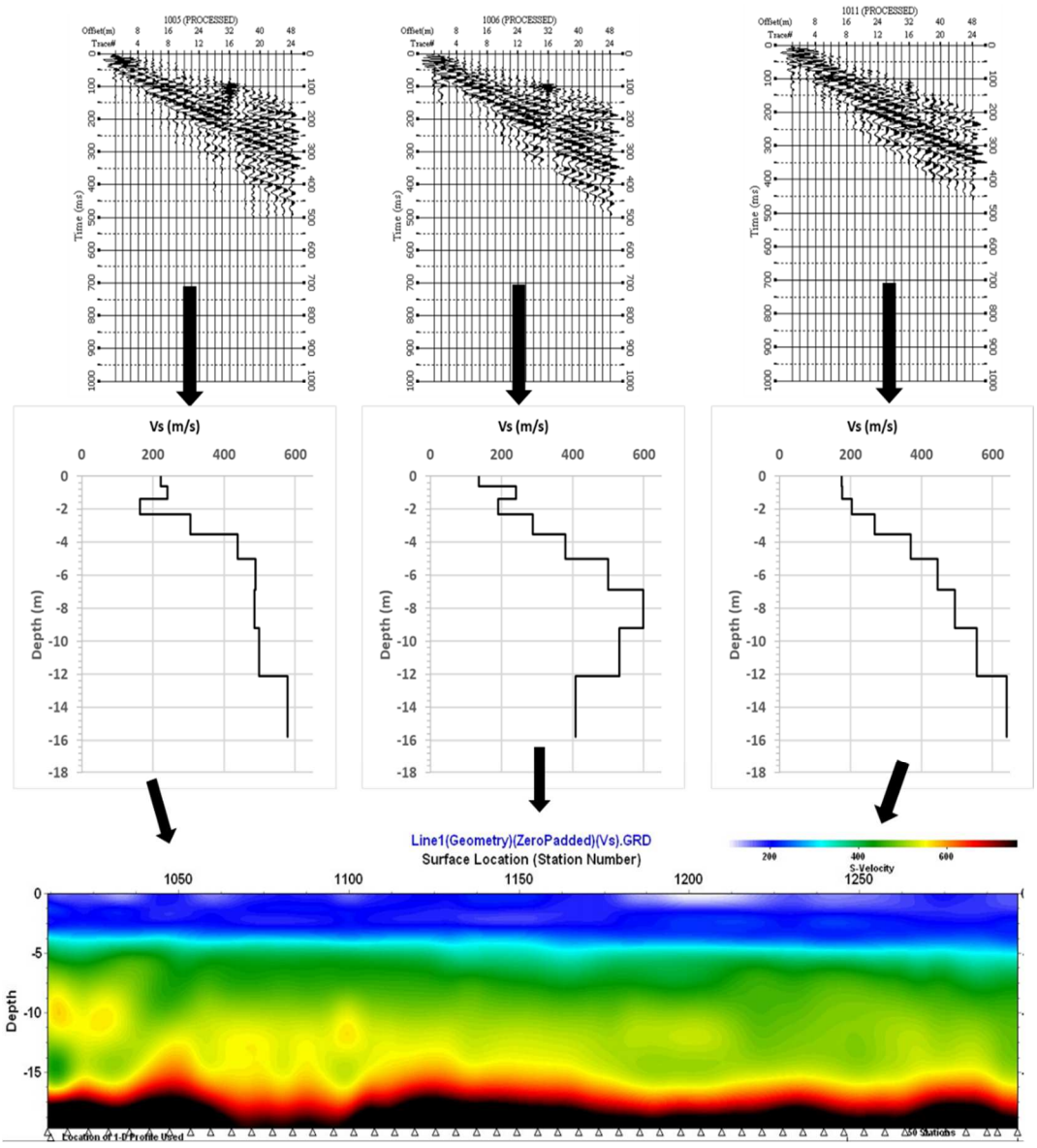

Figure 11: Interpolating multiple 1D Vs models to generate 2D Vs cross section.

Seismic P-wave refraction

The seismic P-wave refraction data were processed using the SeisImager software. The Pickwin™ and Plotrefa™ modules in SeisImager were used for the processing and inversion of the refraction data. The Pickwin module was used to identify and pick the first breaks (Fig. 12). The picked first breaks were then saved as input for the analysis in

the Plotrefa module. The Plotrefa module is basically the interpretation module of SeisImager. Two types of inversion process (time-term inversion and tomographic inversion) were performed on the refraction data using the Plotrefa module.

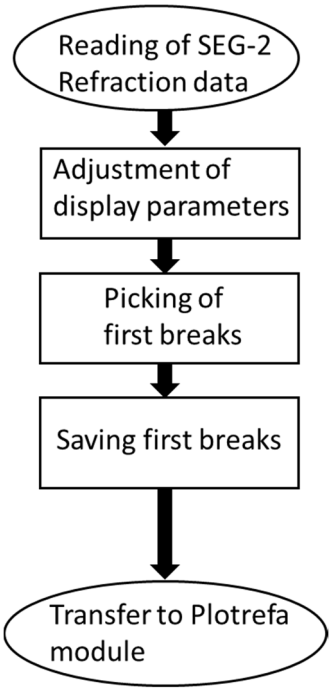

Figure 12: The general flow of Pickwin module of the SeisImager software used to pick the seismic first arrivals.

The steps involved in time-term inversion are shown in Figure 13. The time-term inversion uses linear least-squares and the analysis of delay time for the inversion of first arrivals to produce a velocity model. Assumptions that are part of this inversion technique include that the subsurface is vertically stratified and that no lateral changes in velocity exist. In this inversion, the travel times are plotted against offset, and the change in slope in the plot is used to estimate the depths to the top of the underlying layers. Layers are then assigned in the travel time vs offset plot and the refraction are inverted for velocity section.

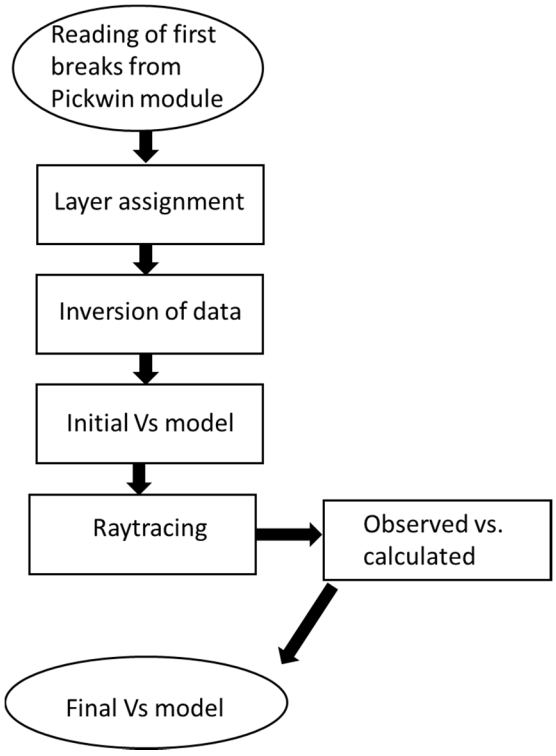

Figure 13: Flow chart showing the steps involved in the time-term inversion of the picked seismic first arrivals.

Figure 14 shows the steps for the tomographic inversion of refraction data. The velocity model generated from the time-term inversion is used as the initial model for the tomographic inversion. The inversion technique generates the layered velocity model by iteratively using raytracing of the initial model to reduce the root mean square error between the calculated and observed travel times.

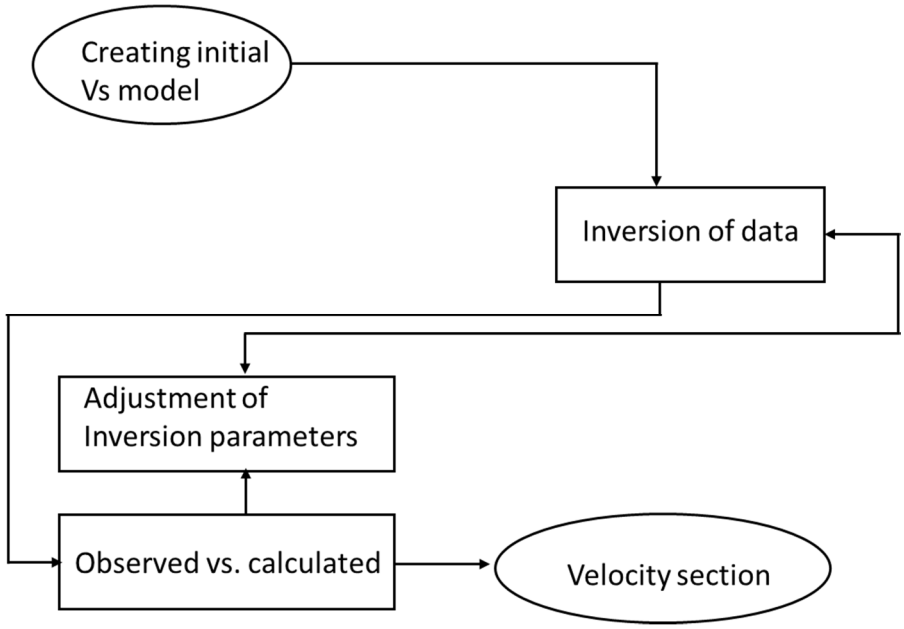

Figure 14: Flow chart showing the steps of the tomographic inversion of the picked first arrivals.

Seismic P-wave reflection

The processing steps applied to P-wave reflection data are shown in Figure 15. Sources and receivers location information were assigned to the file headers according to the acquired data geometry. Trapezoid bandpass filters were applied to mitigate the low-frequency noises and improve the P-wave signal quality. To reduce the amplitude contrast of the traces, an automatic gain control (AGC) with a window of 100 milliseconds (ms) was applied resulting in a significant increase in signal-to-noise ratio. After removing the ground roll from the P-wave data using the surface wave noise attenuation module (SWNA), F-K filtering was applied to remove the remaining ground roll linear noise. Stacking velocities were estimated from velocity analysis of the sorted common mid-point gathers. To remove random noise, enhance the lateral continuity of the stacked sections, and balance the trace amplitude laterally, a frequency-distance (F-X)

filter of Weiner Levinson type was applied to the stacked data. After stacking, the time profiles were converted to depth using smoothed stacking velocity fields.

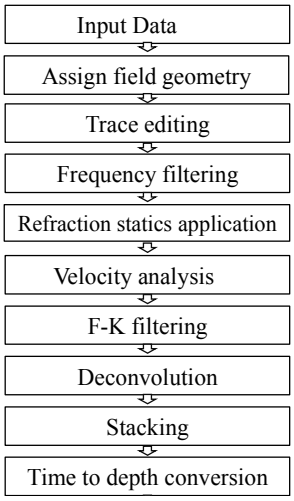

Figure 15: The processing steps of P-wave reflection data.

ERT Data Processing

The apparent resistivity data obtained from the OhmMapper were processed and inverted using RES2DINV (Loke, 1996). The smoothness-constrained Gauss-Newton least-squares inversion technique was used in the inversion (Loke and Barker, 1996; Sasaki, 1992). The subsurface is divided into rectangular blocks to produce a 2D resistivity model followed by optimizing the inversion parameters for better inversion of the ERT data. The optimized inversion parameters include vertical/horizontal flatness filter ratio, damping factor, the number of iterations and convergence limit. The RES2DINV code calculated the values of the apparent resistivity using a finite difference method. The calculated apparent resistivity values were then compared with the measured field data. The resistivity of the model was then tuned in a repetitive manner until the measured

resistivity matched the observed resistivity. The root mean square error was used to quantify the variation of the measured verses the calculated resistivity model. A pseudo-section is then produced from the software. This pseudo-section represents the 2-D distribution of the calculated apparent resistivities, and an inverse model section.

CHAPTER V

DATA INTERPRETATION

The acquired five P-wave reflection seismic profiles, four in northwest Quapaw Oklahoma and one west of the town of Picher Oklahoma were processed to generate P-wave reflection, refraction and MASW images in addition to common-offset displays. The seismic images and the electrical resistivity images generated from the OhmMapper survey are interpreted with the aid of available geological information and mining maps. The interpretation of the five geophysical lines are provided in the section below:

Survey Line 1

Prior to the interpretation of the stacked P-wave reflection profiles, the common-offset displays of each line (example shown in Figure 16) were inspected to detect any disturbance the coherency of the seismic reflection or the surface wave signals that may indicate locations of potential voids. Figure 16 shows disturbed seismic signals near the left and right sides of each profile as indicated by red vertical arrows. There seems to be a delay in the arrival time, which is most likely caused by lower velocity zones at these specific locations, indicating locations of potential voids. These locations are further investigated along the stacked geophysical profile. The vertical resolution of the stacked

profiles in Figure 18a was estimated based on a dominant frequency of 50 Hz (Fig. 17), and an estimated P-wave velocity of 1700 m/s at the target depth for line 1 to be about 8 m according to the quarter wavelength criteria (Yilmaz, 2001). Although the size of the targeted mining voids may be below the vertical resolution seismic reflection images, changes in coherency, arrival time and amplitudes of the reflection signals were used to detect locations of potential voids.

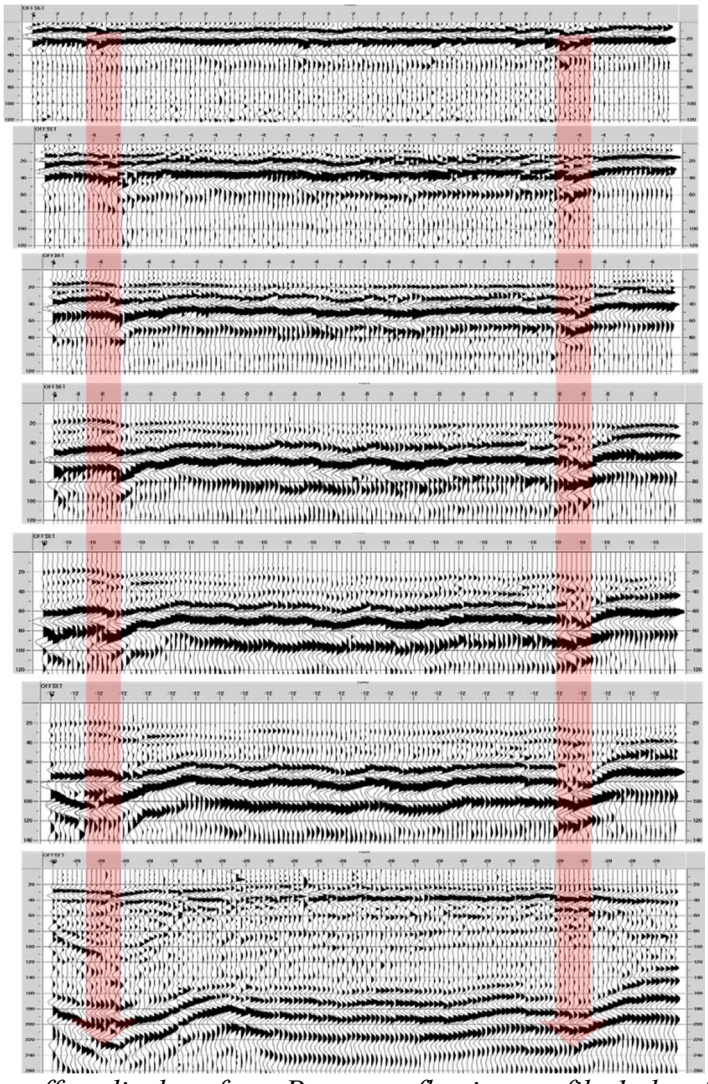

Figure 16. Common-offset displays from P-wave reflection profile 1 showing disturbed seismic signals indicated by red arrows. These disturbed areas may indicate locations of potential voids.

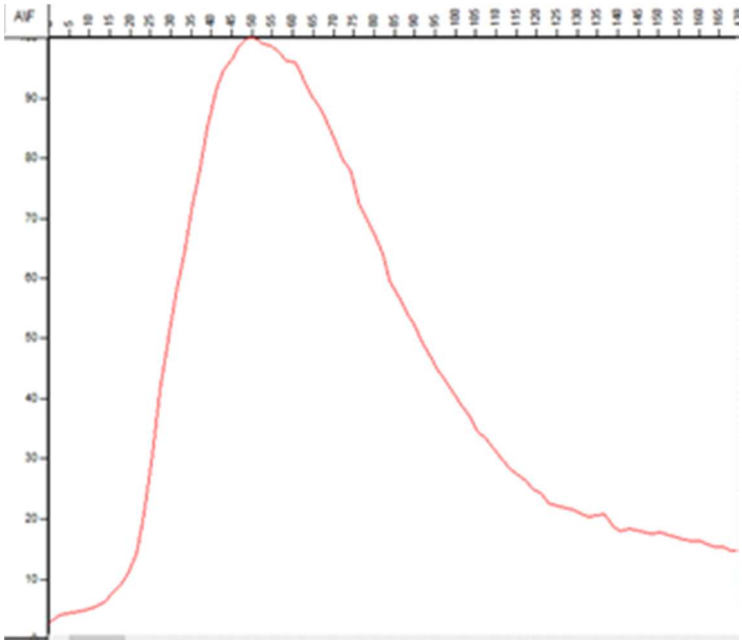

Figure 17: The amplitude spectrum of the stacked seismic Line 1 showing a dominate frequency at 50 Hz

The P-wave reflection profile (Fig. 18a) imaged the subsurface to a maximum depth of 100 m. The profile shows three almost flat, strong and coherent seismic reflectors, which likely correspond to the tops of the Batesville sandstone, Hindsville limestone and Boone Chert Formations, respectively. The top 10 m along the seismic line 1 corresponds to the overburden including soil, clay and mud. A sudden break in the seismic reflector represented the top of the Boone Formation was identified between distance marks 50 and 75 m along the seismic profile 1 (Figure 18a) marking the place of a potential 25 m width mining void located at an average of 40 m depth in the subsurface. The curved reflectors filling the identified void may indicate that the void is partially filled with sediments.

Two other features were observed between distance marks 155 and 165 m, and 240 and 260 m along the seismic profile where the amplitude of the top of the Boone Formation reflector was significantly degraded. The two features are interpreted as locations of potential voids of 15 and 40 m width respectively. These smaller voids seem to have been collapsed as evidenced by the downward shift of the seismic reflectors corresponding to the overlying layers. The feature (marked green on figure 18a) was also delineated below the Boone Formation, and interpreted as a potential ore deposit that have not been mined.

The seismic refraction line 1 (Fig. 18c) imaged the subsurface to a depth of 20 m with velocity ranging from 800 to 4000 m/s. The seismic refraction profile shows three seismic layers. The first layer is 5 m thick and has velocity ranging from 800 to 1700 m/s. This layer corresponds to the interpreted overburden, including soil, clay and mud, from the seismic reflection line 1. The second layer has velocity between 2400 and 3200 m/s and may correspond to the Batesville sandstone The third layer has velocity between 3300 to 4000 m/s and may correspond to the chert limestone of the Boone Formation. A low velocity feature was observed at distance marks 50 to 100 m at 15 m depth along the seismic refraction line 1 (Figure 18c). This feature is located above the interpreted void along the seismic P-wave reflection line (at ~ 40 m depth) and may confirm the collapse of this deeper void. The P-wave refraction line did not detect the other two smaller voids interpreted along the P-wave reflection line (Fig. 18d).

The MASW line 1 imaged the subsurface to a maximum depth of ~ 25 m (Fig. 18d) showing two seismic velocity layers with shear wave velocity (Vs) ranging from 200 to 1500 m/s. The first layer is ~12 m thick and has Vs between 200 and 600 m/s. This layer

is interpreted as the overburden including soil, sands and mud. The high Vs within the interpreted overburden (Vs = 800 m/s) may be due to the variation in the degree of compaction. The second seismic layer occurs at 12 m depth and may correspond to the top part of the chert limestone bedrock. A low-velocity zone is observed at distance mark 40 and 55m, which falls within the identified large void delineated in both the seismic P-wave reflection and P-wave refraction profiles.

In an attempt to track the near surface signature of the interpreted voids in the subsurface, we acquired capacitively coupled resistivity data along the seismic reflection line 1 (Fig. 18b). The ERT profile imaged the upper 11 m in the subsurface which corresponds to the interpreted overburden along the seismic reflection line 1 and the top of Fayetteville Shale. The ERT-1 shows heterogeneous resistivity along the profile and did not show any evidence of subsurface voids along this profile. The heterogeneity of the resistivity values long ERT-1 may be due to difference in moisture as well as variation in the degree of compaction of the overburden.

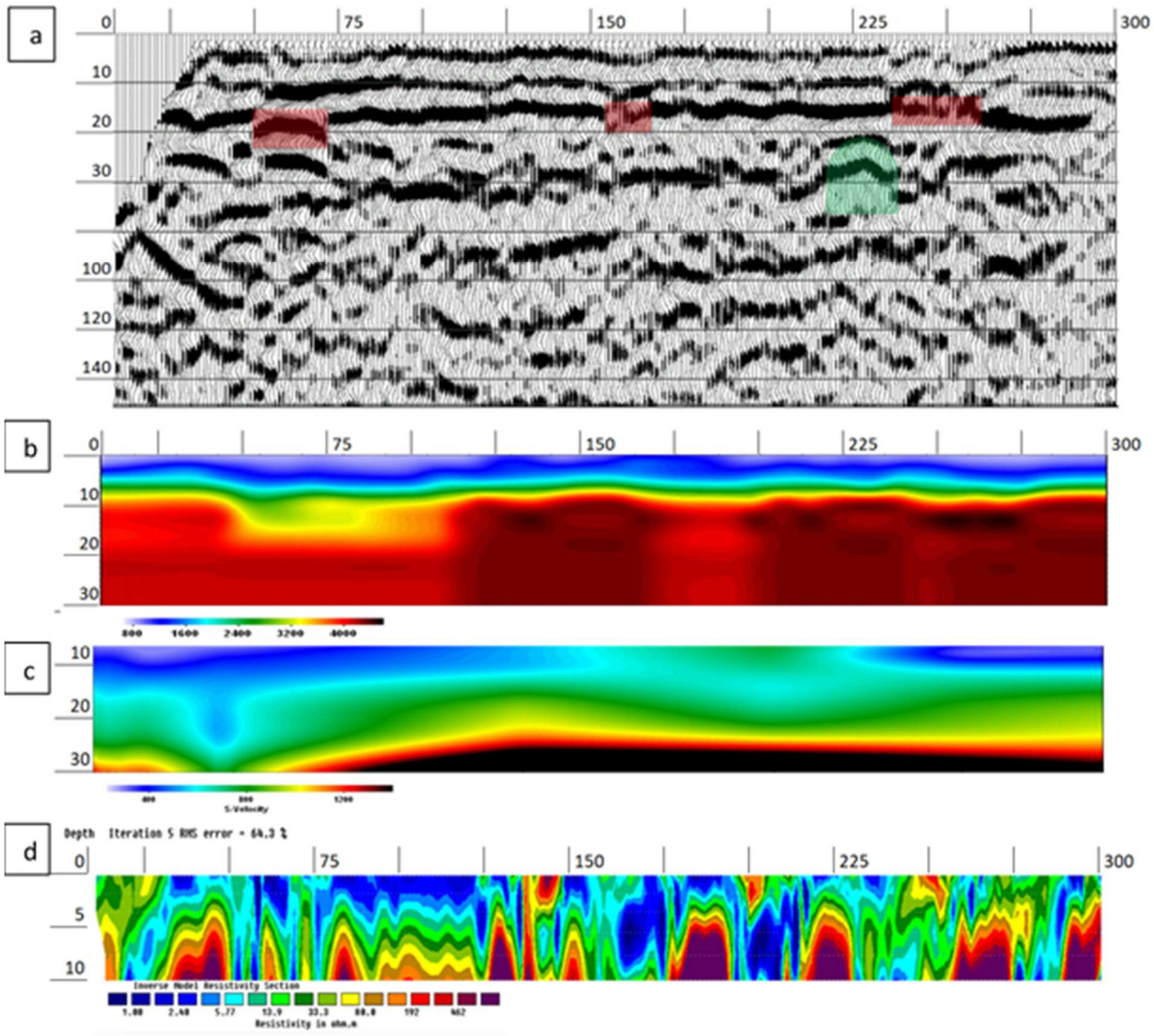

Figure 18: (a) P-wave seismic reflection (b) Seismic Refraction (c) MASW (d) Capacitively coupled ERT

Survey Line 2

The vertical resolution of the stacked profiles in Figure 20a was estimated based on a dominant frequency of 70 Hz (Fig. 19), and an estimated P-wave velocity of 1700 m/s at the target depth for line 1 to be about 6 m according to the quarter wavelength criteria (Yilmaz, 2001).

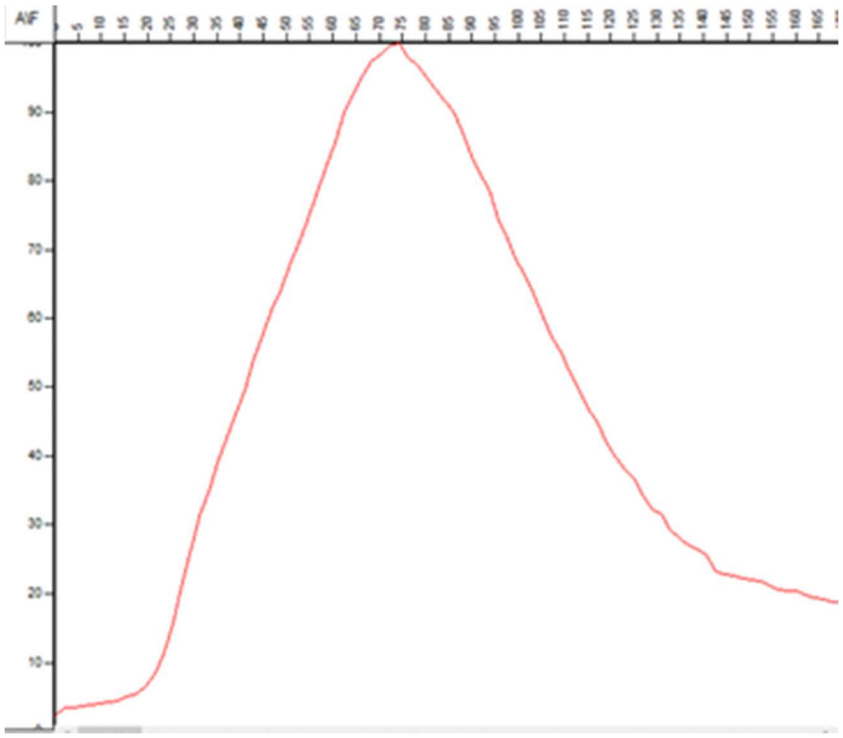

Fig. 19: The amplitude spectrum of the stacked seismic Line 2 showing a dominate frequency at 70 Hz

The P-wave reflection profile (Fig. 20a) imaged the subsurface to a maximum depth of 100 m showing three almost flat, strong and coherent seismic reflectors, which, again, likely correspond to the tops of the Batesville Sandstone, Hindsville Limestone and Boone Formations respectively. The top 10 m along the seismic line 2 corresponds to the overburden. A break in the seismic reflector represented the top of the Boone Formation was identified between distance marks 200 and 220 m along the seismic profile 2 (Figure

20a) marking the location of a potential 20 m width mining void located at an average of 35 m depth in the subsurface. The matching reflectors in the overlying layers may indicate that this void has collapsed and the younger strata above have moved downward into the void. No other features of note were interpreted in this profile.

The seismic refraction line 1 (Fig. 20b) imaged the subsurface to a depth of 20 m with a velocity ranging from 800 to 4000 m/s. The seismic refraction profile shows three seismic layers. The first layer is 8 m thick and has a velocity ranging from 800 to 1700 m/s. This layer corresponds to the interpreted overburden from the seismic reflection line 1. The second layer has a velocity between 2400 and 3200 m/s and may correspond to the Batesville sandstone. The third layer is the Boone Formation and has a velocity between 3300 to 4000 m/s. This layer may correspond to the chert limestone bedrock. No low-velocity feature was observed at distance marks 0 to 20 m at 15 m depth along the seismic refraction line 2 (Figure 20b). This feature is located above the outside the interpretable region of the seismic P-wave reflection line, though may hint at the collapse of an unseen void.

The MASW line 1 imaged the subsurface to a maximum depth of ~ 25 m (Fig. 20c) showing two seismic velocity layers with shear wave velocity (Vs) ranging from 200 to 1500 m/s. The first layer is ~12 m thick and has Vs between 200 and 600 m/s. This layer is interpreted as overburden. The high Vs within the interpreted overburden (Vs = 800 m/s) may be due to the variation in the degree of compaction. The second seismic layer occurs at 12 m depth and may correspond to the top part of the chert limestone bedrock. A low-velocity zone is observed at distance marks 0 and 20m, which falls within the identified large void delineated in the P-wave refraction profile.

Again an attempt was made to track the near-surface signature of the interpreted voids in the subsurface, we acquired capacitively coupled resistivity data along the seismic reflection line 1 (Fig. 20a). The ERT profile imaged the upper 11 m in the subsurface which corresponds to the interpreted overburden along the seismic reflection line 2 and the top of the Fayetteville Shale. The ERT-1 shows heterogeneous resistivity along the profile and did not show any evidence of subsurface voids along this profile. The heterogeneity of the resistivity values along ERT-1 may be due to differences in moisture as well as variation in the degree of compaction of the overburden.

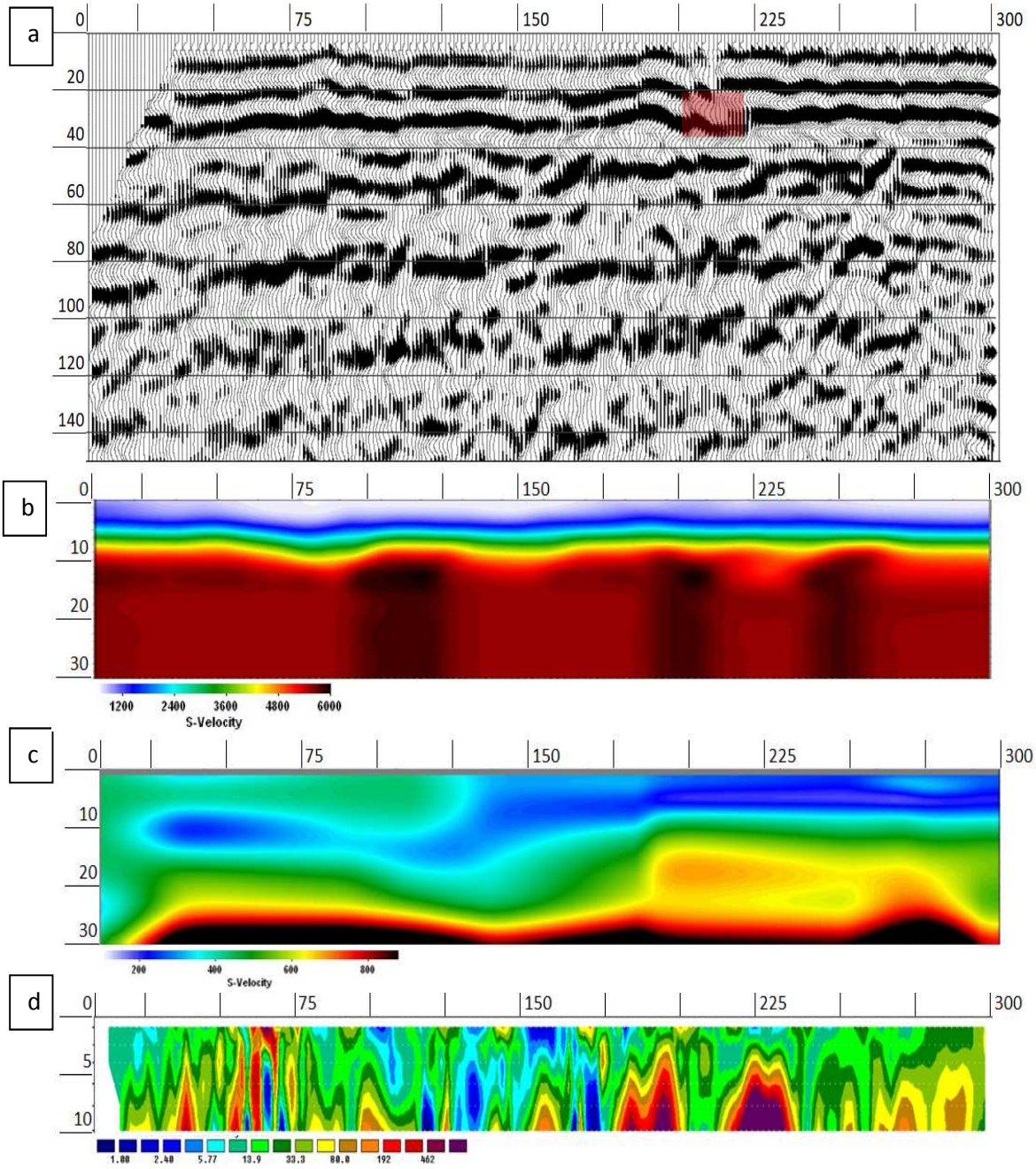

Figure 20: (a) P-wave seismic reflection (b) Seismic refraction (c) MASW (d) Capacitively coupled ERT

Survey Line 3

The vertical resolution of the stacked profiles in Figure 22a was estimated based on a dominant frequency of 70 Hz (Fig. 21), and an estimated P-wave velocity of 1700 m/s at the target depth for line 1 to be about 6 m according to the quarter wavelength criteria (Yilmaz, 2001).

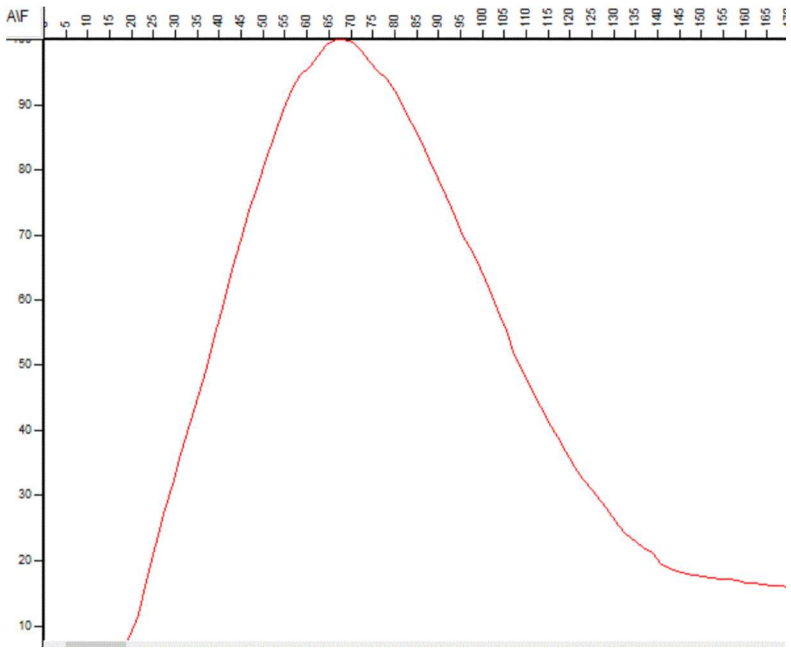

Fig. 21: The amplitude spectrum of the stacked seismic Line 3 showing a dominate frequency at 70 Hz

The P-wave reflection profile (Fig. 22a) imaged the subsurface to a maximum depth of 100 m showing three almost flat, strong and coherent seismic reflectors, which likely correspond to the tops of the Batesville Sandstone, Hindsville Limestone and Boone Formations respectively. The top 10 m along the seismic line 3 corresponds to the overburden. A sudden break in the seismic reflector represented the top of the Boone Formation was identified between distance marks 170 and 210 m along the seismic profile 3 (Figure 22a) marking the place of a potential 40 m width mining void located at

an average of 40 m depth in the subsurface. The curved reflectors filling the identified void may indicate that the void is partially filled with sediments. One feature (marked green on figure 22a) was also delineated below the Boone Formation, and interpreted as potential ore deposits.

The seismic refraction line 3 (Fig. 22b) imaged the subsurface to a depth of 20 m with velocity ranging from 800 to 4000 m/s. The seismic refraction profile shows three seismic layers. The first layer is 5 m thick and has velocity ranging from 800 to 1700 m/s. This layer corresponds to the interpreted overburden from the seismic reflection lines. The second layer has velocity between 2400 and 3200 m/s and may correspond to the Batesville Sandstone. The third layer is the bedrock and has velocity between 3300 to 4000 m/s. This layer may correspond to the chert limestone bedrock. A low-velocity feature was observed at distance marks 0 to 20 m at 15 m depth along the seismic refraction line 3 (Figure 22b). There is no feature on this refraction profile that corresponds to the features interpreted on the seismic reflection profile.

The MASW line imaged the subsurface to a maximum depth of ~ 25 m (Fig. 22a) showing two seismic velocity layers with shear wave velocity (Vs) ranging from 200 to 1500 m/s. The first layer is ~12 m thick and has Vs between 200 and 600 m/s. This layer is interpreted as the overburden. The high Vs within the interpreted overburden (Vs = 800 m/s) may be due to the variation in the degree of compaction. The second seismic layer occurs at 12 m depth and may correspond to the top part of the chert-rich limestone bedrock. The MASW profile shows no substantial low-velocity zones.

Capacitively coupled resistivity data were acquired along the seismic reflection line 3 (Fig. 24a). The ERT profile imaged the upper 11 m in the subsurface which corresponds to the interpreted overburden along the seismic reflection line 3 and the top of the Fayetteville Shale. The ERT-1 shows heterogeneous resistivity along the profile and did not show any evidence of subsurface voids. The heterogeneity of the resistivity values along ERT-3 may be due to difference in moisture as well as variation in the degree of compaction of the overburden.

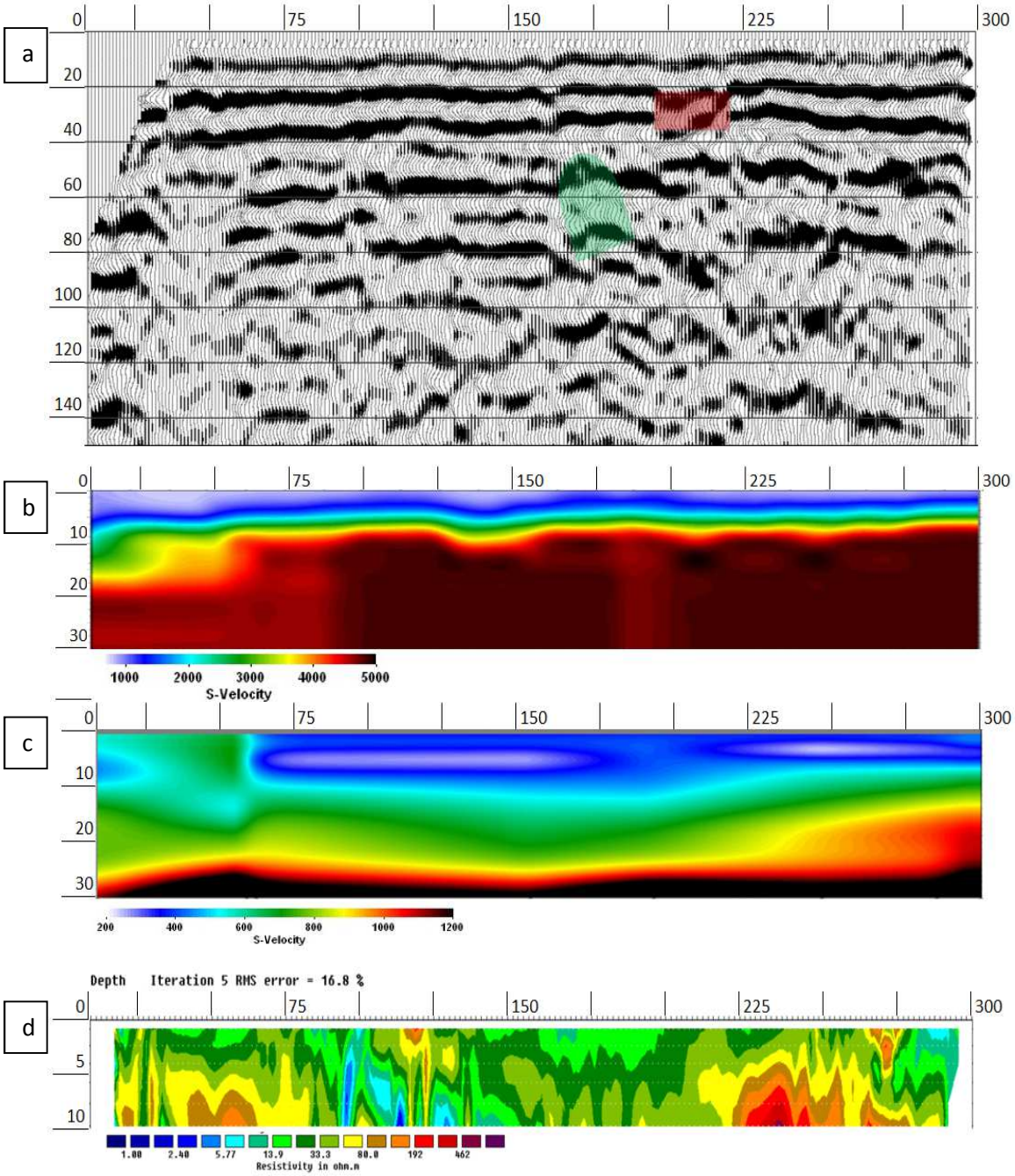

Figure 22 (a) P-wave seismic reflection (b) MASW (c) MASW (d) Capacitively coupled ERT

Survey Line 4

We used the dominant frequency of 65 Hz and velocity of 1700 m/s to estimate the seismic resolution of line 4 (Fig. 23). The estimated seismic resolution is of 6.5 m based on the dominant frequency of 70 Hz and an estimated seismic velocity of 1800 m/s at the target depth

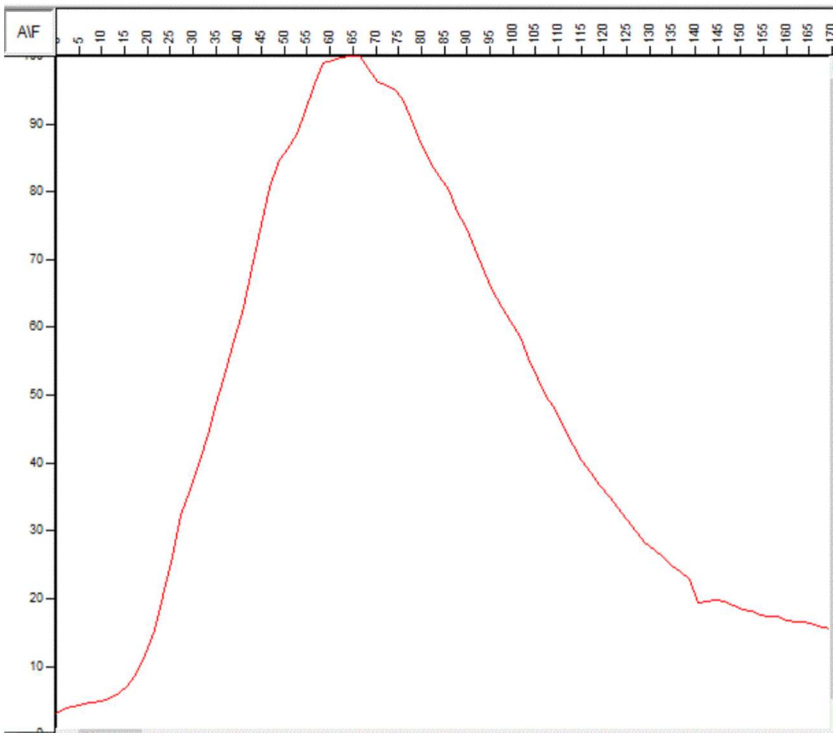

Figure 23: The amplitude spectrum of the stacked seismic Line 4 showing a dominate frequency at 65 Hz.

The seismic reflection line 4 (Fig. 24a) shows three very distinct strong and coherent seismic reflectors. These seismic reflectors are interpreted to correspond to the top of the Batesville Sandstone, Hindsville Limestone and Boone Formation, respectively. The top layer along this seismic line is interpreted to be overburden. Three features at distance marks 100, 125, and 140 were delineated along the seismic line 4 at the top of the

interpreted Boone Formation. The delineated features are interpreted to be potential voids, occurring at depth 40 m. Strata above these voids appear to have collapsed as observed by the downward shift of the diffraction event. Another event was identified at distance marks 200 and 225 m (marked green), occurring at 60 m depth. This event is interpreted to be an unmined ore body.

The seismic P-wave refraction line 4 (Fig. 24b) imaged the subsurface to a depth of 15 m. Three seismic velocity layers were delineated by the seismic line 4 with Vp ranging from 900 to 5000 m/s. The first layer is about 5 m thick and has Vp ranging from 900 to 2000 m/s; interpreted as the overburden. The second layer has Vp between 2200 and 3800 m/s and may be interpreted as shale based on the geology of the study area. The third layer has Vp ranging from 3900 to 5000 m/s. This layer may be interpreted as the cherty limestone. There is no evidence of voids on the seismic P-wave refraction line 4.

The MASW line 2 (Fig. 24a) imaged the subsurface to a depth of 15 m. Two seismic layers are delineated along MASW line 4 with Vs ranging from 150 to 900 m/s. The first layer is 5 m thick and has Vs between 150 and 400 m/s. This layer also corresponds to the overburden. The second layer has Vs ranging from 500 to 800 m/s and is interpreted as the cherty limestone bedrock. There is a distortion between the first layer and the second layer at distance marks 80 and 150. The distortion appears to correspond to the location of the void delineated by the seismic reflection profile 4, and may thus be due to collapsed voids in the subsurface.

The capacitively coupled resistivity data along this line imaged the subsurface to a depth of 11 m and generally shows two geoelectric layers with varying resistivity values from

13 to 500 Ωm (Fig. 24b). The first geoelectric layer corresponds to the interpreted overburden with resistivity between 13 and 33 Ωm. The second geoelectric layer has higher resistivity ranging from 80 to 500 Ωm and may correspond to the bedrock. A feature (blue circle) with low resistivity was identified at distance mark 80 and 150 within the bedrock. This feature corresponds to the location of interpreted voids in the seismic reflection line and thus may be due to the presence of void in the subsurface.

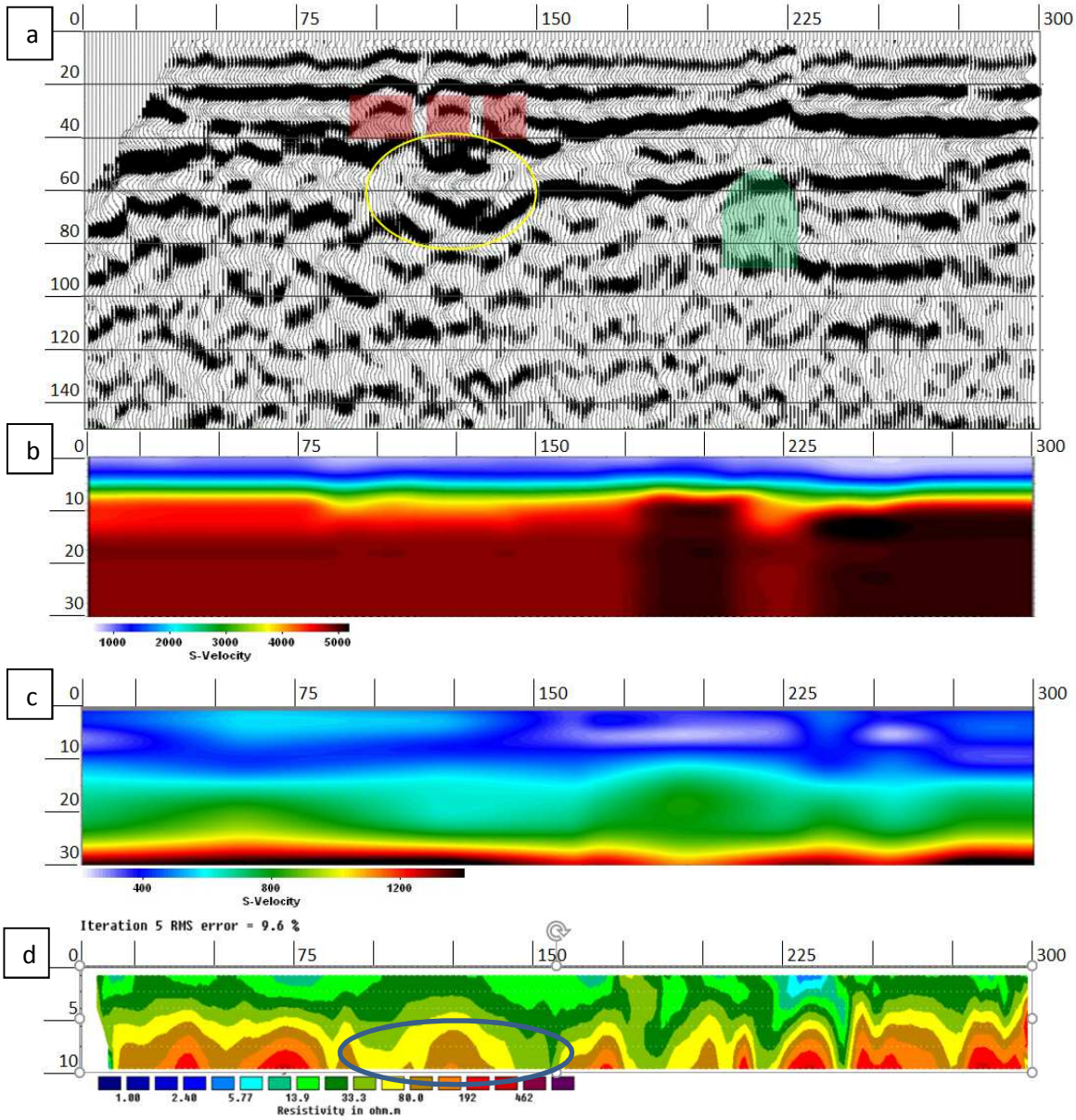

Figure 24. (a) P-wave seismic reflection (b) Seismic offsets (c) MASW (d) Capasitivly coupled ERT

Survey Line 5

Figure 26a, Line 5, was taken at a separate location from the previous 4 lines. This data was acquired at a location west of Picher, Oklahoma over a known mapped void space from Luza (1986). The estimated seismic resolution is 5.25 m using a dominant frequency of 80 Hz and a velocity of 1700 m/s (Fig. 25)

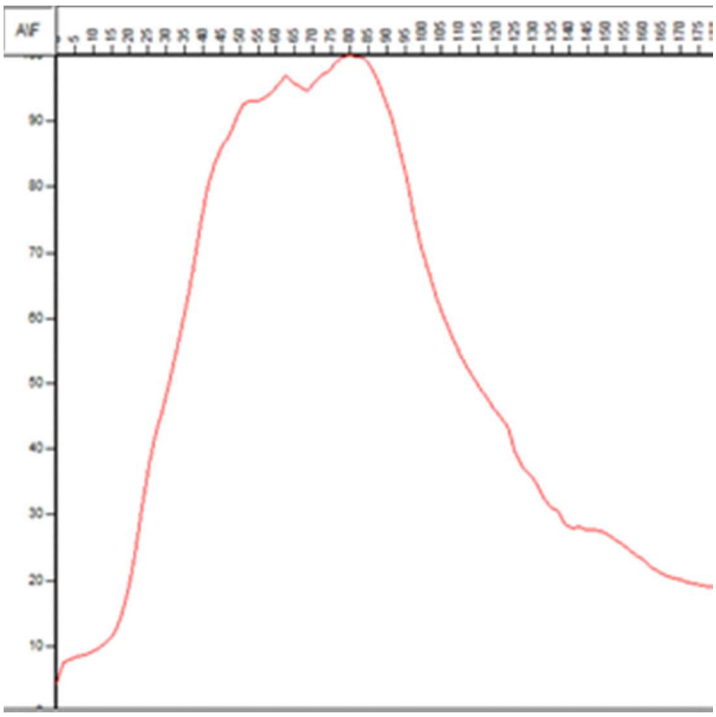

Figure. 25: The amplitude spectrum of the stacked seismic Line 5 showing a dominate frequency at 80 Hz

The P-wave reflection profile (Fig. 26a) imaged the subsurface to a maximum depth of 100 m showing three almost flat, strong, and coherent seismic reflectors, which likely correspond to the tops of the Batesville Sandstone, Hindsville limestone and Boone Formations respectively. At the very top of the profile, the Fayetteville Shale is just starting to show up as a weak reflector. The top 10 m along the seismic line 4

corresponds to overburden. A sudden break in the seismic reflector represented the top of the Boone Formation was identified between distance marks 140 and 170 m along the seismic profile 4 (Figure 26a) marking the place of a potential 30 m width mining void located at an average of 45 m depth in the subsurface. A second break in the seismic reflector was identified between marks 230 and 250 marking the place of a potential 30 m width mining void located at an average of 30 m depth in the subsurface. One feature (marked green on figure 26a) was also delineated below the Boone Formation and interpreted as a potential ore deposit that has not been mined.

The seismic refraction line 4 (Fig. 26b) imaged the subsurface to a depth of 20 m with a velocity ranging from 800 to 4000 m/s. The seismic refraction profile shows three seismic layers. The first layer is 8 m thick and has a velocity ranging from 800 to 1700 m/s. This layer corresponds to the interpreted overburden from the seismic reflection line 4. The second layer has a velocity between 2400 and 3200 m/s and may correspond to the Batesville Sandstone. The third layer is the bedrock and has a velocity between 3300 to 4000 m/s. This layer may correspond to the cherty limestone of the Boone Formation. The P-wave refraction line did not detect the voids interpreted along the P-wave reflection line.

The MASW line 4 imaged the subsurface to a maximum depth of ~ 25 m (Fig. 26c) showing two seismic velocity layers with shear wave velocity (Vs) ranging from 200 to 1500 m/s. The first layer is ~12 m thick and has Vs between 200 and 600 m/s. This layer is interpreted as overburden. The high Vs within the interpreted overburden (Vs = 800 m/s) may be due to the variation in the degree of compaction. The second seismic layer

occurs at 12 m depth and may correspond to the top part of the chert and limestone. The MASW line did not detect the voids interpreted along the P-wave reflection line.

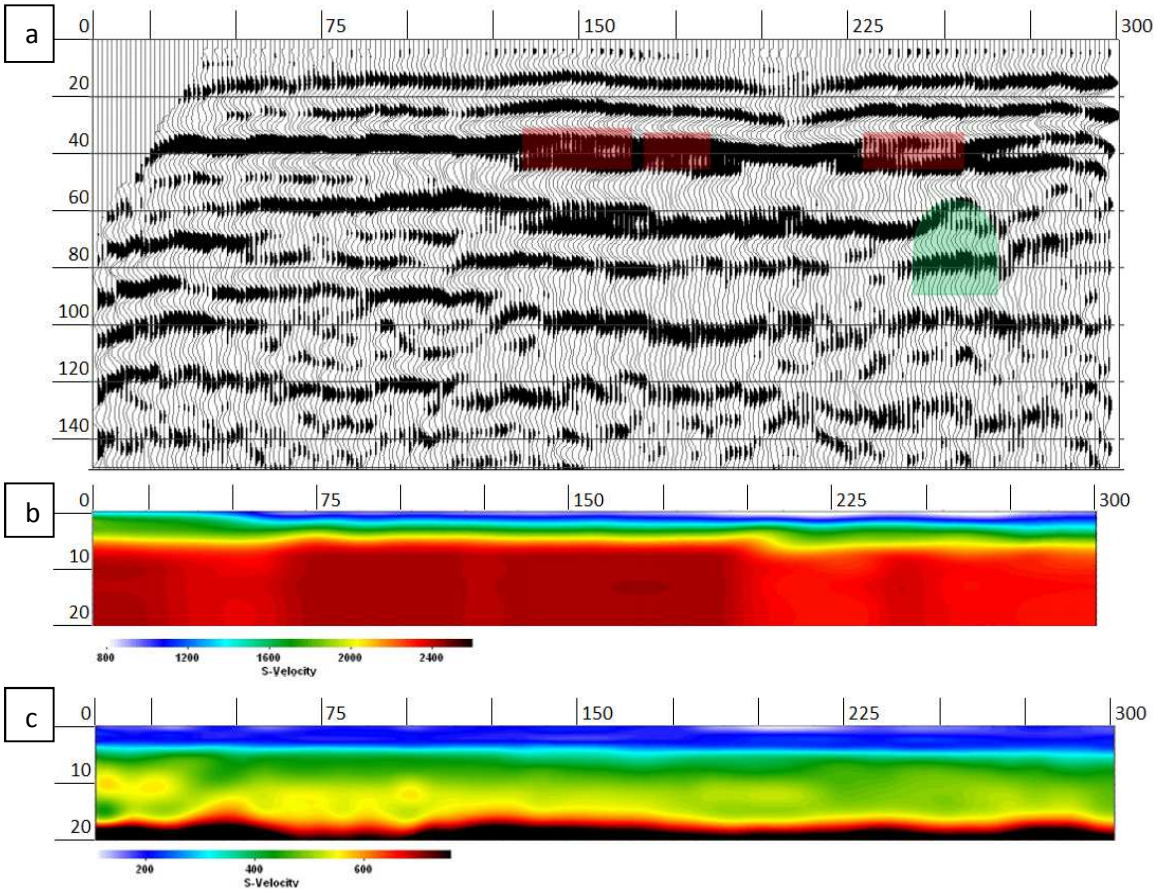

Figure 26. (a) P-wave seismic reflection, (b) Seismic refraction and (c) multichannel analysis of surface wave.

CHAPTER VI

DISCUSSION AND CONCLUSIONS

The aim of this research was to evaluate the use of selected geophysical methods that can be employed in environments where surface conditions are less than ideal. One of the more challenging locations for all geophysical methods is urbanized areas. Urbanized areas often contain large noise sources as well as ground conditions that make using most geophysical methods extremely difficult or impossible. Likewise, with more geophysical work being done in environmental engineering and remediation at brown sites and superfund sites, health and safety concerns can become a larger factor in geophysical data collection planning. In this case, data collection speed as well as minimizing the number of individuals necessary becomes more important.

A series of seismic surveys were conducted at two locations: in Quapaw Oklahoma and west of Picher Oklahoma. These surveys were processed into reflection, refraction and MASW profiles for the purpose of evaluating the P-wave seismic land streamer as a tool for rapid, noninvasive data collection. Seismic data collected from these lines were processed into P-wave reflection, P-wave Refraction, and MASW profiles. These profiles were interpreted and probable voids were noted.

These P-wave seismic survey lines were matched with ERT data collected with the use of a Geometrics OhmMapper. The ERT data was processed in RES2DINV into profiles for interpretation. The majority of data collected was found to be of too poor quality to be used for interpretation purposes. Due to the nature of the OhmMapper system it is unknown if this is the result of environmental noise, user error, an issue in the system itself, or a combination of all three. The Geometrics OhmMapper system proved to be less useful at this site than the seismic land streamer. However, this system does deserve more investigation in terms of usefulness.

The p-wave seismic land streamer proved to be capable of producing quality results relatively quickly and efficiently with a small team and no disturbance to the surface soil. The seismic data collected were of sufficient quality to be processed into reflection, refraction, and multichannel analysis of surface wave (MASW). P-wave reflection profiles were able to locate anomalies that were interpreted as voids as well as potential ore bodies. P-Wave Refraction, while not being able to penetrate deep enough to directly image voids in this region, in cases where a void has caused the overlying rock and overburden to shift and reduce competency, a void can be inferred. These results are matched in the MASW profiles. Once again when a void shifts allowing the overlying structures to shift as well this change in the subsurface is expressed in the MASW profiles.

REFERENCES

Astor, M. (2017, August 7). Florida Sinkhole Claims Five More Homes. The New York Times. https://www.nytimes.com/2017/08/07/us/florida-sinkhole.html

Belfer, I., I. Bruner, S. Keydar, A. Kravtsov, and E. Landa, 1998, Detection of shallow objects using refracted and diffracted seismic waves: Journal of Applied Geophysics, 38, 155–168.

Bharti, A. K., Pal, S. K., Priyam, P., Pathak, V. K., Kumar, R., & Ranjan, S. K. (2016). Detection of illegal mine voids using electrical resistivity tomography: the case-study of Raniganj coalfield (India). Engineering Geology, 213, 120-132.

Brockie, D. C.; Hare, E. H., Jr.; and Dingess, P. R., 1968, The geology and ore deposits of the Tri-State District of Missouri, Kansas, and Oklahoma, in Ridge, J. D., editor, Ore deposits of the

Chai, H., K. Phoon, S. Goh, and C. Wei, 2012, Some theoretical and numerical observations on scattering of Rayleigh waves in media containing shallow rectangular cavities: Journal of Applied Geophysics, 83, 107– 119, doi: 10.1016/j.jappgeo.2012.05.005.

Chen, D. H., & Scullion, T. (2008). Detecting subsurface voids using ground-coupled penetrating radar. Geotechnical Testing Journal, 31(3), 217-224.

Corvette Cave In Exhibit. (2021). National Corvette Museum. https://www.corvettemuseum.org/explore/exhibits/corvette-cave-in-exhibit/

Di Fiore, V., Angelino, A., Passaro, S., & Bonanno, A. (2013). High resolution seismic reflection methods to detect near surface tuff-cavities: A case study in the Neapolitan area, Italy. Journal of Cave and Karst Studies, 75(1), 51-59.

Fowler, G. M., and J. P. Lyden, 1932, The ore deposits of the Tri-State District (Missouri, Kansas, Oklahoma):American Institute of Mining and Metallurgical Engineers, Technical Publication 446, Class I, Mining Geology, No. 39, p. 49.

Geometrics, 2001, OhmMapper TR1 Operation Manual rev. F: San Jose, Calif., Geometrics, Inc., accessed Aug 2020 at geom.geometrics.com/pub/GeoElectric/Manuals/OhmMapper-Manual-TRN-2004.PDF

Geometrics, Inc. (2018). *OhmMapper Resistivity Mapper*. Geometrics OhmMapper. Retrieved November 22, 2021, from https://geometrics.com/wp-content/uploads/2018/10/OhmMapper_Spec_Sheet.pdf.

Grandjean, G., and D. Leparoux, 2004, The potential of seismic methods for detecting cavities and buried objects: Experimentation at a test site: Journal of Applied Geophysics, 56, 93–106, doi: 10.1016/j.jappgeo.2004.04 .004.

Hartley-Parkinson, R. (2019, August 14). Amiens sinkhole threatens to swallow pub into secret medieval cave. Metro. https://metro.co.uk/2019/08/14/amiens-sinkhole-threatens-swallow-pub-secret-medieval-cave-10567092/

Hermann, A. (2018, August 11). Sinkhole opens at Tanger Outlets in Lancaster, swallowing multiple cars. PhillyVoice.

Ivanov, J., R. D. Millser, C. B. Park, and N. Ryden, 2003, Seismic search for underground anomalies: 73rd Annual International Meeting, SEG, Expanded Abstracts, 1223–1226, doi: 10.1190/1.1817502.

Johnson, W. J., Snow, R. E., & Clark, J. C. (2002, October). Surface geophysical methods for detection of underground mine workings. In Symposium on Geotechnical Methods for Mine Mapping Verifications, Charleston, West Virginia, October (Vol. 29).

Keydar, S., M. Mikenberg, V. Shtivelman, and I. Rochlin, 2016, Imaging shallow linear diffractors by 3D weighted multipath summation: 78th Annual International Conference and Exhibition, EAGE, Extended Abstracts, doi: 10.3997/2214-4609.201600986.

Landa, E., and S. Keydar, 1998, Seismic monitoring of diffraction images for detection of local heterogeneities: Geophysics, 63, 1093–1100, doi: 10 .1190/1.1444387.

McCann, D. M., R. Baria, P. D. Jackson, M. G. Culshaw, A. S. P. Green, D. L. Suddaby, and J. R. Hallam, 1982, The use of geophysical methods in the detection of natural cavities, mineshafts and anomalous ground conditions: Report of the Engineering Geology Unit, Institute of Geological Sciences, No. EG/82/15.

McKnight, E. T.; and Fischer, R. P., 1970, Geology and ore deposits of the Picher field, Oklahoma and Kansas:U.S. Geological Survey Professional Paper 588, p. 165.

Miller, R. D., and Steeples, D. W. (1991). Detecting voids in a 0.6 m coal seam, 7 m deep, using seismic reflection. Geoexploration, 28(2), 109-119.

Morton, S. L. C., S. L. Peterie, J. M. Ivanov, R. D. Miller, and S. D. Sloan, 2017, Joint interpretation of multi-component surface wave data for tunnel detection: 87th Annual

International Meeting, SEG, Expanded Abstracts, 5458–5464, doi: 10.1190/segam2017-17675948.1.

Nobes, D. C. (2017). Ground penetrating radar response from voids: A demonstration using a simple model. Ndt & E International, 91, 47-53.

Peterie, S. L., R. D. Miller, and D. W. Steeples, 2009, Diffraction imaging versus reflection processing for shallow void detection: 79th Annual International Meeting, SEG, Expanded Abstracts, 1421–1424, doi: 10 .1190/1.3255115.

Peterie, S. L., and R. D. Miller, 2015, Near surface scattering phenomena and implications for tunnel detection: Interpretation, 3, no. 1, SF43–SF54, doi: 10.1190/INT-2014-0088.1.

Riddle, G. I., C. J. Hickey, and D. R. Schmitt, 2010, Subsurface tunnel detection using electrical resistivity tomography and seismic refraction tomography: A case study: SAGEEP Proceedings, 552–562.

Reed, E. W.; Schoff, S. L.; and Branson, C. C., 1955, Ground-water resources of Ottawa County, Oklahoma: Oklahoma Geological Survey Bulletin 72, p. 203.

Samyn, K., A. Bitri, and G. Grandjean, 2013, Imaging a near-surface feature using cross-correlation analysis of multi-channel surface wave data: Near Surface Geophysics, 11, 1–10, doi: 10.3997/1873-0604.2012007.

Schneider, F. M., S. Esterhazy, I. Perugia, and G. Bokelmann, 2017, Seismic resonances of acoustic cavities: Geophysical Prospecting, 65, 1–24, doi: 10.1111/1365-2478.12523.

Shao, G., G. P. Tsoflias, and C. Li, 2016, Detection of near-surface cavities by generalized S-transform of Rayleigh waves: Journal of Applied Geophysics, 129, 53–65, doi: 10.1016/j.jappgeo.2016.03.041.

Sheets, R. A. (2002). Use of electrical resistivity to detect underground mine voids in Ohio (Vol. 2, No. 4041). US Department of the Interior, US Geological Survey.

Sherman, C. S., J. Rector, D. Dreger, and S. Glaser, 2018, A numerical study of surface-wave-based tunnel detection at the Black Diamond Mines Regional Preserve, California: Geophysics, 83, no. 4, EN13–EN22, doi: 10.1190/geo2017-0467.1.

Siebenthal, C. E., 1908, Lead and zinc, Mineral resources of northeastern Oklahoma, in Metals and non-metals, except fuels, pt. 1 of Contributions to economic geology, 1907: U.S. Geological Survey Bulletin 340, p. 187-228.

Sloan, S. D., S. L. Peterie, R. D. Miller, J. Ivanov, J. T. Schwenk, and J. R. McKenna, 2015, Detecting clandestine tunnels using near-surface seismic techniques: Geophysics, 80, no. 5, EN127–EN135, doi: 10.1190/ geo2014-0529.1.

United States. Army. Corps of Engineers. Tulsa District ;Oklahoma., Subsidence Evaluation Team, & Office of the Secretary of Environment. (2006, January). PICHER MINING FIELD, NORTHEAST OKLAHOMA SUBSIDENCE EVALUATION

REPORT (W1700.3 P592s 2006 85765750). Oklahoma Secretary of the Environment. http://www.swt.usace.army.mil/LIBRARY/libraryDetail.cfm?ID=208

Walters, S. L., Miller, R. D., & Xia, J. (2007). Near-surface tunnel detection using diffracted P-waves: A feasibility study. In SEG technical program expanded abstracts 2007 (pp. 1128-1132). Society of Exploration Geophysicists.

Walters, S. L., R. D. Miller, D. W. Steeples, J. Xia, and C. Zeng, 2009, Detecting tunnels and underground facilities using diffracted P-waves: SAGEEP Proceedings, 937–942.

Walters, S., Miller, R., Xia, J., Ivanov, J., Steeples, D., & Zeng, C. (2009, March). Detecting tunnels and underground facilities using diffracted P-waves. In 22nd EEGS Symposium on the Application of Geophysics to Engineering and Environmental Problems (pp. cp-157). European Association of Geoscientists & Engineers.

Weidman, Samuel; Williams, C. F.; and Anderson, C. O., 1932, The Miami-Picher zinc-lead district, Oklahoma: Oklahoma Geological Survey Bulletin 56, p. 177.

Xia, J., J. E. Nyquist, Y. Xu, M. J. S. Roth, and R. D. Miller, 2007, Feasibility of detecting near-surface feature with Rayleigh-wave diffraction: Journal of Applied Geophysics, 62, 244–253, doi: 10.1016/j.jappgeo .2006.12.002.

Zahari, M. N. H., Madun, A., Dahlan, S. H., Joret, A., Abidin, M. Z., Mohammad, A. H., & Omar, A. H. (2018, April). Experimental Detection and Characterization of Void using Time-Domain Reflection Wave. In Journal of Physics: Conference Series (Vol. 995, No. 1, p. 012102). IOP Publishing.

Zeng, C., J. Xia, R. D. Miller, and G. P. Tsoflias, 2009, Modeling results on detectability of shallow tunnels using Rayleigh-wave diffraction: 79th Annual International Meeting, SEG, Expanded Abstracts, 1425–1429, doi: 10.1190/1.3255116.

VITA

Patrick Meese

Candidate for the Degree of

Master of Science

Thesis: LOCATING UNMAPPED MINING VOIDS USING HIGH-RESOLUITION SEISMIC AND RESISTIVITY SURVEYS AT A HISTORICAL MINING AREA IN THE TRI-STATE MINING DISTRICT, QUAPAW OKLAHOMA

Major Field: Geology

Biographical:

Education:

Completed the requirements for the Master of Science in your major at Oklahoma State University, Stillwater, Oklahoma in December, 2021

Completed the requirements for the Bachelor of Science in your major at Oklahoma State University, Stillwater, Oklahoma in 2019.